JOURNAL OF GEOPHYSICAL RESEARCH, VOL. 91, NO. B12, PAGES 12,539-12,571, NOVEMBER 10, 1986

MOST RECENT ERUPTION OF THE MONO CRATERS, EASTERN CENTRAL CALIFORNIA

Kerry Sieh and Marcus Bursik

Division of Geological and Planetary Sciences, California Institute of Technology, Pasadena

Abstract. The most recent eruption at the Mono Craters occurred in the fourteenth century A.D. Evidence for this event includes 0.2 km^3 of pyroclastic fall, flow, and surge deposits and 0.4 km^3 of lava domes and flows. These rhyolitic deposits emanated from aligned vents at the northern end of the volcanic chain. Hence we have named this volcanic episode the North Mono eruption. Initial explosions were Plinian to sub-Plinian events whose products form overlapping blankets of air fall tephra. Pyroclastic flow and surge deposits lie upon these undisturbed fall beds within several kilometers of the source vents. Extrusion of five domes and coulees, including Northern Coulee and Panum Dome, completed the North Mono eruption. Radiocarbon dates and dendrochronological considerations constrain the eruption to a period between A.D. 1325 and 1365. The lack of lacustrine laminae or aeolian and fluvial beds between individual pyroclastic beds suggests that the explosive phases of the eruption took place over a period of not more than several months. Within the resolution of the available radiocarbon and dendrochronologic dates, the North Mono eruption is contemporaneous with the latest eruption of the Inyo volcanic chain, about 20 km to the south. However, the Inyo tephra blanket clearly overlies, and thus postdates, all North Mono tephra. Minor disturbance of the North Mono tephra prior to deposition of the Inyo tephra indicates that the period of time between the North Mono and Inyo eruptions was probably no more than a year or two. This near contemporaneity of the two eruptions suggests a genetic relationship. Liquefaction of North Mono sands on the floor of Mono Lake occurred twice during the waning stages of the North Mono eruption and 3 times immediately before and after pulses of the Inyo eruption. This is evidence that five earthquakes of $M_L > 5.5$ occurred during the North Mono and Inyo eruptions. The chemical and textural similarity of the erupted products and their nearly simultaneous evacuation from aligned vents indicates that the North Mono eruption resulted from intrusion of a dike beneath the northern 6 km of the volcanic chain. Several observations suggest that dike intrusion beneath the Mono Craters has replaced normal faulting as the mechanism for elastic rebound and permanent extension of the crust at this latitude. However, dike widths compatible with relief of purely tectonic strains (<3 m) are probably too narrow to have allowed the North Mono magma to erupt. Overpressurization of the Mono Craters magma reservoir by another mechanism, perhaps magma mixing, appears necessary as well. The gradually diminishing explosiveness of the North Mono eruption probably resulted from a decrease of water content downward in the dike. The pulsating nature of the early, explosive phase of the eruption may represent the repeated rapid drawdown of slowly rising vesiculated magma to about the saturation depth of the water within it.

Paper number 6B5929.
0148-0227/86/006B-5929$05.00

Introduction

Several dozen silicic eruptions have occurred along the tectonically active eastern flank of the central Sierra Nevada within the past 35,000 years; many of these eruptions have, in fact, occurred within the past 2000 years. This violent, exciting, and youthful past suggests an interesting future and encouraged us to undertake this study of the timing and nature of one of the most recent eruptions.

The most recent period of volcanic activity in this region began about 3 m.y. ago with widespread outpourings of basalt and andesite and more local extrusions of quartz latite [Bailey et al., 1976]. Between 2.1 and 0.8 m.y. ago, many cubic kilometers of high-silica rhyolite were erupted from centers to the southeast [Metz and Mahood, 1985]. The most voluminous and explosive eruption in the region occurred about 0.7 m.y. ago. At that time, the evacuation of some 600 km^3 of high-silica rhyolite from a subterranean chamber produced subsidence of the Long Valley caldera (Figure 1) and the widespread dispersal of air fall and pyroclastic flow deposits [Bailey et al., 1976; Izett and Naeser, 1976; Hildreth and Mahood, 1986].

In the 0.7 m.y. subsequent to the climactic caldera-forming event, many smaller eruptions of basaltic to rhyolitic magma have occurred within the western half of the caldera [Bailey et al., 1976]. Seismic and geodetic activity within and south of the caldera since 1978 appears, in fact, to be related to modern movement of magma or other fluids beneath the caldera (see summary of recent investigations by Hill et al. [1985]).

The youngest manifestation of volcanic activity on the eastern flank of the central Sierra Nevada is a chain of craters and silicic flows that extends 40 km northward from Long Valley caldera to Mono Lake. This zone of recent activity comprises the volcanos of Mono Lake, the domes and flows of the Mono Craters, the Inyo domes and craters, and the phreatic explosion pits of Mammoth Mountain (shown in black in Figure 1). These youthful features have attracted the attention of geologists for over a century. Earlier investigations include those of Russell [1889], Mayo and others [1936], Putnam [1938], Rinehart and Huber [1965], Kistler [1966] and Huber and Rinehart [1967].

The oldest known pyroclastic products from the chain are the rhyolitic air fall beds found throughout 35,000- to 12,000-year-old lacustrine

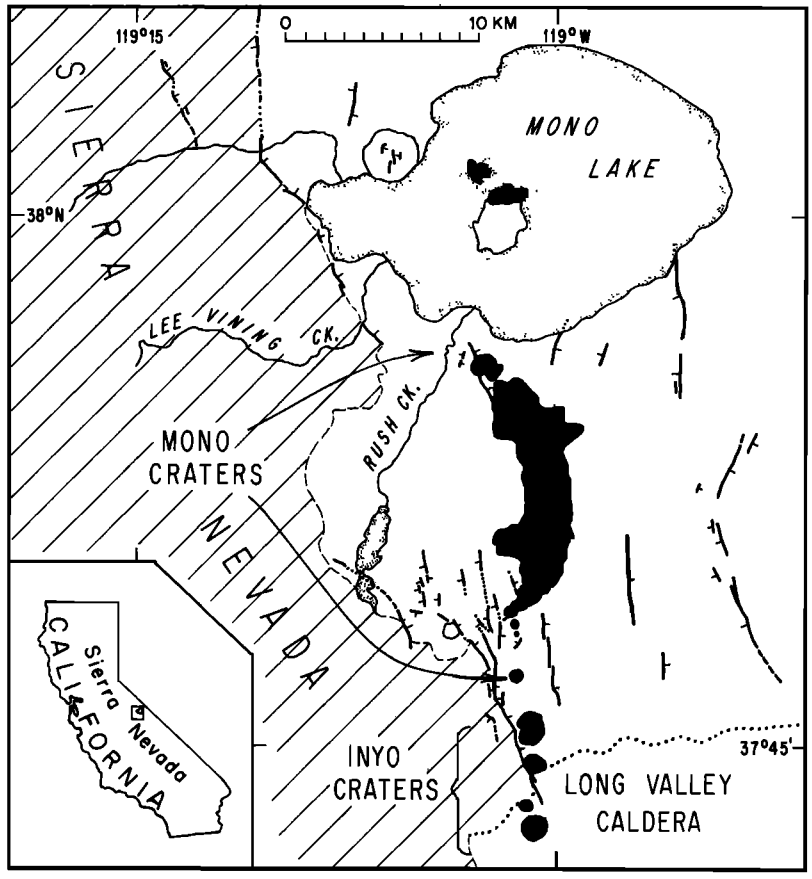

Fig. 1. The Mono and Inyo craters and volcanoes of Mono Lake (in black) form a 40-km-long chain of Late Pleistocene and Holocene craters, domes, and flows which have been emplaced along the tectonically active eastern flank of the Sierra Nevada. Pattern of latest Pleistocene and Holocene faults is from our unpublished mapping.

beds around Mono Lake [Lajoie, 1968; Lajoie and Robinson, 1982]. Wood [1977a, 1984] estimated the oldest exposed domes to be about 35,000 years old.

Most of the young domes, flows, and craters between Mammoth Mountain and Mono Lake are Holocene in age. Using obsidian hydration-rind thicknesses calibrated by one radiocarbon date, Wood [1977a, 1984] estimated ages of 10,000 to 640 years for all but four of the 24 currently exposed domes and flows of the Mono Craters. All the Inyo domes and craters have formed during the Holocene epoch [Miller, 1985], and Stine [1984] has shown that the volcanic islands of Mono Lake are less than 1800 years old. The dacitic lavas and minor pyroclastic beds found on the northern flank of Paoha, the larger of the two principal islands, were erupted during the youngest known eruption in the region, no more than about 200 years ago.

Products of the Eruption

We have divided the products of the most recent eruption of the Mono Craters into three groups, on the basis of their timing and areal extent. As is common to silicic eruptions (see, for example, Williams and McBirney [1979, p. 75] and Fisher and Schmincke [1984, p. 63]), this episode began with its most explosive (Plinian) phase, progressed through a period dominated by pyroclastic flows and surges, and ended with a period during which viscous, block-encrusted lava domes and flows were extruded. The products of the earliest of these three phases are air fall beds that blanket at least 8000 km^2 of the region surrounding Mono Lake. The pyroclastic flow and surge deposits of the second phase are limited to an area of approximately 100 km^2 around the source vents, and the lava domes and flows cover only 6 km^2 in the immediate vicinity of the eruptive vents. These deposits are described below, in the general order of their eruption.

Air Fall Beds

Shallow natural and hand-dug exposures in the region of Mono Lake commonly reveal a distinctive packet of planar, well-sorted ash and lapilli beds. Figures 2 and 3 are photographs of two such exposures; a locality characterized by thick and coarse beds deposited near the source vents is illustrated in Figure 2; a site characterized by a thin set of fine-grained beds deposited far from the source vents is illustrated in Figure 3. Although this series of air fall beds varies markedly in thickness and coarseness, we have been able to correlate the series throughout the region by tracing distinctive individual beds.

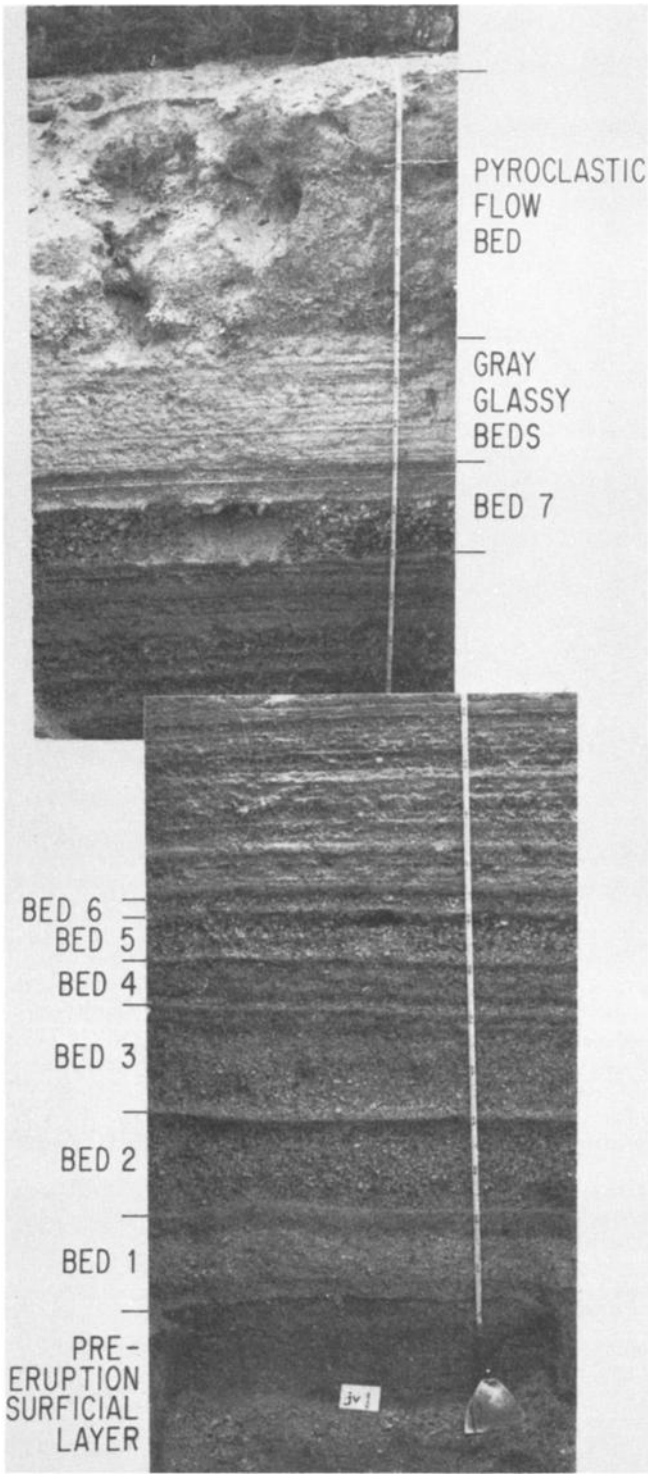

Fig. 2. Photomosaic of the planar-bedded ash and lapilli air fall beds of the latest eruption at site "jv." Total thickness of air fall beds is 2.05 m here. (Numbers on tape are at 10-cm intervals.) Individual beds referred to in text are labeled. This locality, only 1.5-4.0 km from the source vents, in a road cut on the south side of Highway 120, about 420 m east of the intersection of Highway 120 and the State Tufa Reserve Road, is labeled "188" in Figure 5.

The air fall blanket is well preserved where it is thick ($\gtrsim$ 50 cm) and where it was buried soon after deposition. Fortunately, rapid burial (by pyroclastic flows on the plains south of Mono Lake, by clays beneath Mono Lake, by windblown sand northeast of the lake, and by debris flows in the canyons of the Bodie Hills) protected these beds from erosion and bioturbation at numerous informative localities. Thin blankets of the ash left unburied at the surface have been bioturbated by plant roots and organisms or eroded by nonbiological agents.

At sites within several kilometers of the source vents the various air fall beds are composed predominantly of angular, aphyric white lineated pumice, with lesser amounts of gray microvesicular glass and black obsidian. Analyses of obsidian clasts by electron microprobe (S. Newman et al., personal communication, 1985) indicate that all of the air fall beds are high-silica rhyolite. In thin section, opaque microphenocrysts and anhedral grains of biotite and feldspar are rare but present. Clasts of Sierran granitic and metamorphic rock commonly constitute about 1% of bed volume; the well-rounded nature of most of these accidental clasts indicates that the rising magma penetrated and eroded Pleistocene gravels of the Rush Creek delta (Figure 1). Angular fragments of gray, reddish-brown, brown, and black porphyritic accessory volcanic rocks also commonly constitute a percent or so of these beds. These clasts have textures similar to those in the older domes and flows penetrated by some of the conduits and are presumed to be derived from them. Quartz- and sanidine-rich pink angular fragments of the Bishop Tuff, which lies 100-200 m beneath the surface in the area, are also present, but rare, in some of the air fall beds.

Figure 4 is an isopach map of the air fall blanket. For clarity, data points south of 38° latitude are not shown. The isopach contours indicate that the thickest part of the air fall deposit is in the vicinity of two large flows. Most of the beds are also coarsest in this vicinity. Thus the principal source of the air fall beds must be one or more vents in this area along the northern crest of the Mono Craters. Hence we have named this tephra blanket and its associated pyroclastic flow and surge deposits the North Mono tephra.

The air fall component of the North Mono tephra is distributed asymmetrically about its principal sources; most of the tephra lies in the quadrant northeast of the source region (Figure 4). Such asymmetry is commonly observed in air fall blankets, and is usually attributed to winds prevailing at the time of the eruption (for several examples, see Fisher and Schmincke [1984, pp. 132-139]). In this case, the northern to north-northeastern trend of the axis of dispersal indicates that the winds prevailing during the course of the eruption were out of the south and south-southwest. This is not surprising because such winds are dominant in this region during all but the stormy winter season.

The North Mono tephra includes many mappable individual beds which represent distinct and separate eruptions within this latest eruptive

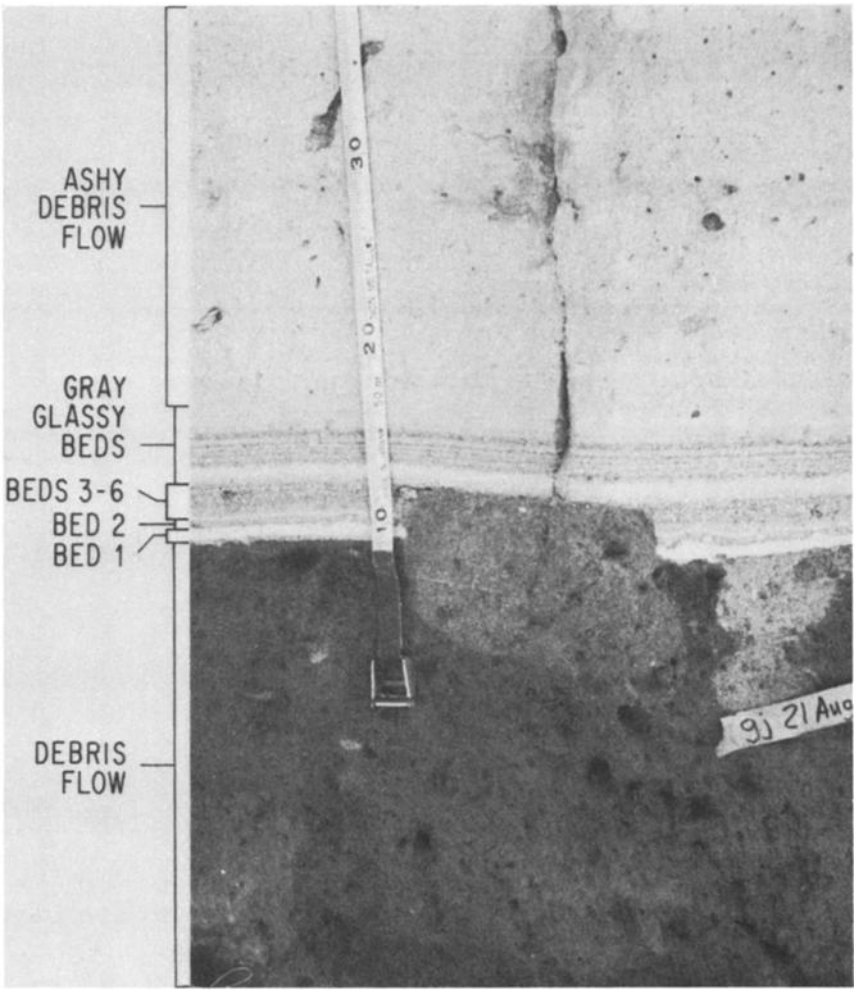

Fig. 3. Photograph of the planar-bedded ashy air fall beds at a locality north of Mono Lake and far from the sources of the eruption. Total thickness of the air fall beds here is only 75 mm. Individual beds referred to in text are labeled. Air fall beds rest upon the massive pebbly loam of a small alluvial fan and are overlain by a debris flow composed of air fall ash and red-brown volcanic pebbles washed off the nearby hillside. This locality, in Cottonwood Canyon, 7.3 km north of Mono Lake, is labeled "gj" in Figure 4. Tape is graduated in centimeters.

episode. The more prominent of these beds are described below.

Bed 1. Bed 1 is the basal unit of the North Mono tephra and contains about 10% of the total air fall volume, the largest percentage of any individual air fall bed in the series. It consists of 80-95% white lineated pumice and is labeled in Figures 2 and 3. The bed covers at least 7000 km^2. Its dispersal index of about 1800 km^2 and fragmentation index of about 50% put it in the Plinian category of Walker [1980]. Prevailing winds out of the southwest throughout the course of the eruption produced an axis of dispersal that trends northeastward (Figures 5 and 6). Normal grading in all exposures indicates a gradual diminution of the height of the Plinian column prior to the cessation of the eruption [Walker, 1980].

Bed 2. Lying upon the sharp upper boundary of bed 1 is another distinctive unit which, for lack of a better imagination, we call bed 2 (Figures 2 and 3). Bed 2 is particularly distinctive in the near field, where its lower two fifths is appreciably darker, owing to a concentration of black obsidian pyroclasts. This distinction is less impressive at far-field sites, where stratigraphic position and thickness are our principal criteria for recognition of the bed.

The isopach maps of this bed (Figures 7 and 8) demonstrate that the Plinian column from which the pyroclasts of bed 2 fell was blown north-northwestward from a source under Upper Dome and blanketed the entirety of Mono Lake. This is the only major fall bed with a dispersal axis directed so far west of north, and thus it is the most prominent air fall bed in excavations west of the longitude of Panum Dome.

Beds 3, 4, 5, and 6. The third episode of the North Mono eruption is represented stratigraphically by beds 3-6 (Figures 2 and 3). In the western half of the tephra blanket, each of these is a distinct, well-sorted bed of white lineated pumice with lesser amounts of dull gray microvesicular glass and black obsidian. In the eastern half of the tephra blanket these beds are united into one reversely graded bed.

The overall northward trend of its dispersal

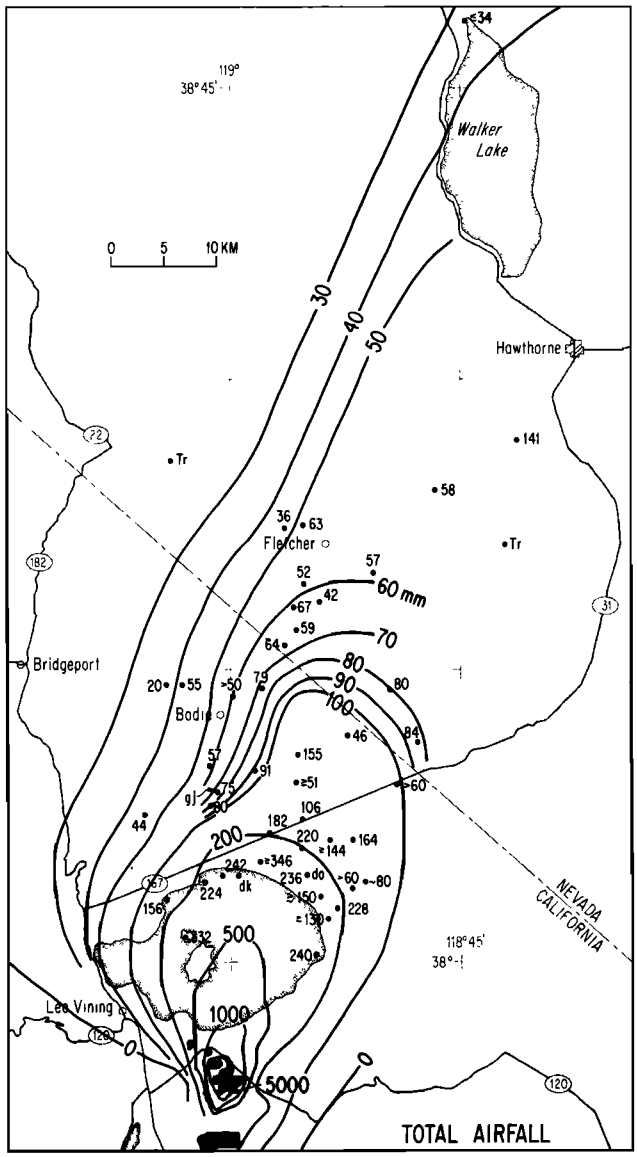

Fig. 4. Known extent and thickness of the air fall beds of the North Mono tephra. This blanket of tephra and its associated pyroclastic flow deposits are called the North Mono tephra because the source vents are located at the north end of the Mono Craters. Volume of these beds is at least 0.42 km^3 (0.17 km^3, dense rock equivalent). All thickness data north of 38°N latitude are shown. Data from localities south of 38°N are available on microfiche (Figure A1). Lava domes and flows (coulees) shown in black are, from north to south, Panum Dome, Cratered Dome, Upper Dome, Northern Coulee, and Southern Coulee. All but Southern Coulee were extruded at the end of the most recent eruption, after deposition of the North Mono Tephra. For reference, the locality illustrated in Figure 2 is about 1 km north of the 5000 m contour on Highway 120, and the locality depicted in Figure 3 is labeled "gj."

axis (Figure 9) indicates that the prevailing winds at the time of the eruption were toward the north. The east-west facies variation is more difficult to explain. The gradational changes in grain size of the bed east of its dispersal axis may well indicate several changes in the height of the Plinian column from which the pyroclasts were falling [Walker, 1980]. Alternatively, wind speed may have increased, or mass eruption rate may have gradually increased [Wilson et al., 1980]. However, the sharp boundaries between beds 3, 4, 5, and 6 west of the dispersal axis suggest four distinct eruptive pulses, the last pyroclasts from each one settling out of the atmosphere before the first pyroclasts of the succeeding pulse were deposited. It is difficult to envision wind patterns that could explain the odd east-west variation in this air fall bed. A more plausible explanation (discussed below) involves simultaneous eruption of the bed from more than one source vent.

Bed 7. Bed 7 is an air fall bed distinguished by its stratigraphic position (Figure 2) and its rich assemblage of accessory and accidental pyroclasts. At all localities the lower 15-50% of the bed is distinctly darker than overlying portions due to an abundance of black, gray, green, red, and lavender pyroclasts. Among these odd pyroclasts are porphyritic glasses as well as red scoriaceous (basaltic?) pyroclasts, banded black and orange glass, and green obsidian pyroclasts. Black, aphyric obsidian and gray microvesicular glass are also common and may represent either juvenile materials or fragments of Northwest Coulee, an older lava flow penetrated by the bed 7 vent. White lineated pumice is present in this darker lower part of bed 7 but is dominant in the upper 50-85% of the bed.

The richness of accidental and accessory pyroclasts among the white juvenile pumice in the lower portion of bed 7 indicates that substantial erosion of the walls of the volcanic conduit occurred during the early phase of this eruptive pulse. The lack of angular granitic debris and rounded Sierran plutonic or metamorphic rocks signifies that conduit erosion occurred only above the level of the Pleistocene delta plain of Rush Creek, within the edifice of the volcanic chain, that is, at depths within the conduit of less than 200 m. The abundance of juvenile white pumice pyroclasts among the accidentals and the occurrence of this darker basal facies of bed 7 even at far-field sites indicates that this conduit erosion took place during a sustained high-energy eruptive pulse. The pumice-dominated upper portions of bed 7 represent the later stages of this eruptive pulse during which conduit erosion had ceased or slowed markedly.

Figure 10a shows that bed 7 was deposited as a markedly asymmetric, narrow blanket extending northeastward into Nevada. The extreme northeastward elongation indicates that winds were exceptionally strong out of the southwest at the time of the eruption. The prominent asymmetry across the dispersal axis probably resulted from a low-level crosswind which blew pyroclasts in a more northwesterly direction during the final few kilometers of their descent. Wood et al. [1986] and Waitt et al. [1981] have shown that divergence of low- and high-level wind azimuths produced a similar effect in the airfall blankets of the 1980 eruptions of Mount St. Helens.

Gray glassy beds. The last widely dispersed air fall unit of the North Mono eruption consists

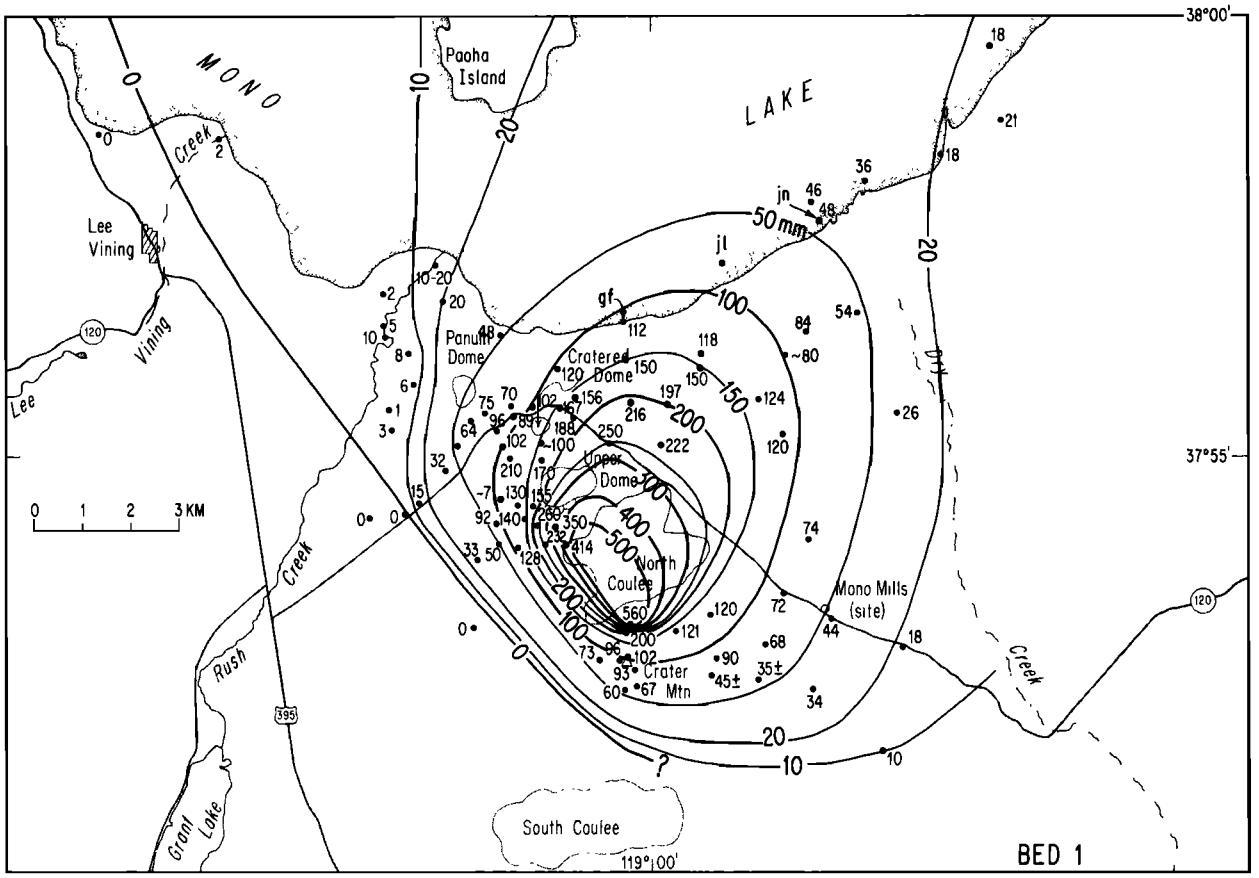

Fig. 5. Isopach map of proximal bed 1 shows that low-level winds were blowing toward the northeast during the eruption of bed 1. The shape of the 500-mm contour shows that bed 1 pyroclasts were evacuated from a linear vent or a northwesterly alignment of vents now buried beneath the southwestern part of Northern Coulee. This and similar maps of other erupted units enable calculation of the volume of erupted magma.

of planar laminated beds dominated by translucent, vitreous, light gray glassy pyroclasts. These beds are unusually fine-grained and poor in pumiceous pyroclasts. This unique textural character notwithstanding, the chemical composition of these gray glassy pyroclasts is indistinguishable from that of the black obsidians in the underlying pumiceous beds (S. Newman et al., personal communication, 1985). Bioturbation and aeolian reworking of this uppermost air fall bed is common, and thus the thickness contours shown on Figure 11 are more irregular. Nevertheless, one can conclude from the thickness map that the majority of the unit was deposited in the quadrant northeast of Northern Coulee. At least part of this unit, however, was blown southward.

Pyroclastic Flows and Surge Deposits

Most exposures within several kilometers of the source vents contain pyroclastic flow deposits, and several reveal pyroclastic surge beds. The known extent of these deposits is shown on Figure 12. Only those three deposits that are geomorphically mappable have been mapped and named. For clarity of presentation, we have chosen to divide the deposits into three groups: (1) those deposited between the eruption of beds 6 and 7, (2) those associated with the gray glassy beds, and (3) those erupted from Panum Crater.

Pyroclastic deposits between beds 6 and 7. At near-field sites northeast of the source vents, numerous thin planar beds rest between beds 6 and 7 (see, for example, Figure 2). Some of these beds are as well sorted as, but much thinner than, beds 1-6; these are air fall beds so minor that they commonly are not correlable between more than a few exposures. Other thin beds are planar but are so poorly sorted that an air fall origin seems unlikely. Thicknesses of these lapilli-rich ash beds, which occur up to at least 4 km from the source vents, range from a few millimeters to about 7 cm. The beds are massive and do not rest upon erosional contacts. We interpret them to be very minor, highly fluid pyroclastic flows that emanated from sources in the region of Upper Dome and Northern Coulee.

Pyroclastic flows associated with the gray glassy beds. Numerous outcrops in and surrounding the northern half of the Mono Craters expose pyroclastic flow beds closely associated with the gray glassy beds (GGB). Most of these are poorly sorted, moderately compact, pale pink lapilli-rich ash bodies without clear geomorphic boundaries. These deposits must have originated

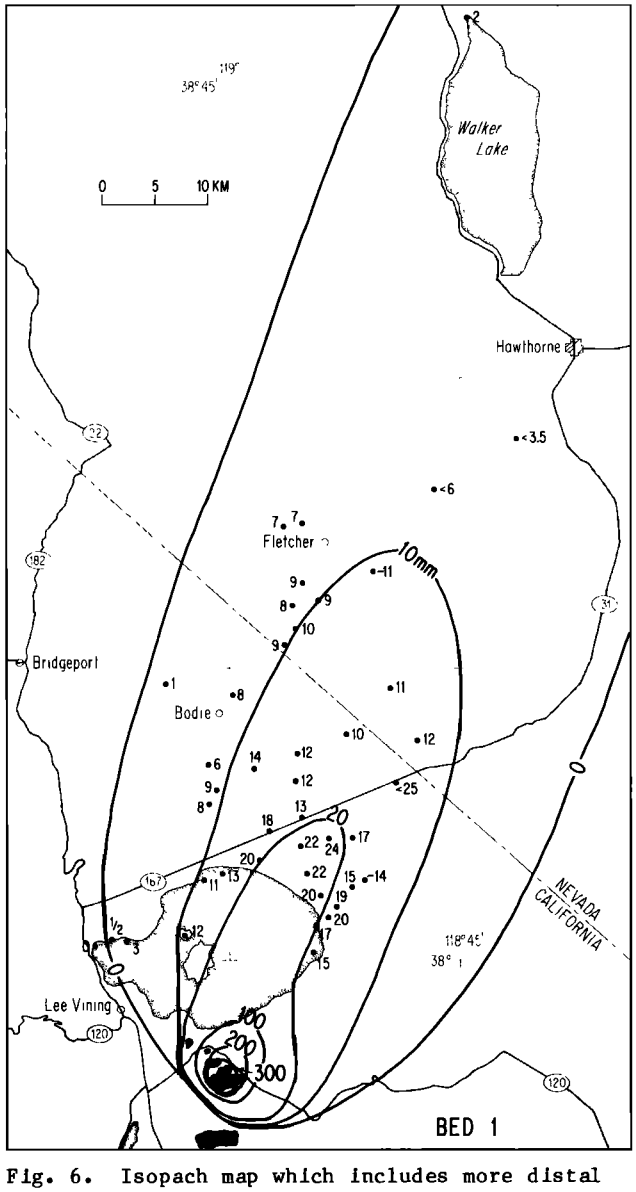

Fig. 6. Isopach map which includes more distal portions of bed 1 shows that prevailing high-level winds at the time of the eruption were also toward the northeast.

as rapidly moving slurries of hot juvenile pyroclastic debris and gas, so fluid that they could taper to thicknesses of only a few centimeters or less at their distal and lateral margins, up to 8 km from source. The complete absence of planar- or cross-bedding in these massive beds also argues against transport of the pyroclasts in highly inflated volcanic clouds or nuées ardentes or as saltating bed load at the base of such clouds.

The oldest recognized flow deposit of this group rests directly upon the basal unit of the GGB (bed 8) at sites "aa" and "ct" (Figure 12). The close association of this flow bed with bed 8 suggests the possibility of a common source vent or vents, somewhere between Upper Dome and Northern Coulee.

Slightly younger massive flow beds are common throughout the area. These flow beds occur within the GGB. Examples include a 2.8-m-thick flow, rich in obsidian blocks, atop hill 8825 immediately south of Northern Coulee on the crest of the range. Site "aa" and nearby pits also contain flow beds intercalated with the GGB. Shallow pits southeast of Northern Coulee exposed a pyroclastic flow bed beneath a meter or more of the GGB, and although the base of this flow deposit was not exposed, we tentatively correlate it to the flows in the middle of the GGB at "aa." A 6-m-deep backhoe excavation at "cp" (just east of the tip of Northern Coulee) revealed the massive uppermost 5 m of a pink pyroclastic flow deposit of undetermined total thickness. This flow deposit is overlain by 1 m of the GGB, and we offer a tentative correlation to the mid-GGB flow at site "aa." This thick flow deposit probably underlies at least the barren sand flat which stretches about 1 km toward the northeast from Northern Coulee and probably underlies most of Northern Coulee as well.

North, west, and east of Cratered Dome, the North Mono tephra is capped by a 0.7-2.3-m-thick pyroclastic flow unit. This massive, lapilli-rich coarse ash bed overlies all GGB deposited at these sites. Figure 2 shows this bed at the top of the exposure at site "jv." At this site, the unit displays variable sorting and has less ash than other pyroclastic flows. These characteristics suggest that the unit may be a lahar or colluvial unit composed of thoroughly churned air fall beds that slid off steep slopes about 0.5 km to the south. The pyroclasts within the unit, however, are larger than those found in air fall units near the proposed source of slumping, and a unit in the same stratigraphic position is found in nearly all other exposures within a kilometer to the north and west. Furthermore, at many of these nearby sites the exposed massive bed is distinctly pale pink or pale orange in color, a common, though not infallible, criterion for distinguishing pyroclastic flow deposits from lahars [Fisher and Schmincke, 1984, p. 211]. This deposit may well correlate with flow beds beneath the uppermost GGB in exposures farther east because the youngest GGB have not been deposited at "jv" and nearby localities. A much more detailed analysis of the GGB stratigraphy will be required to place firmer constraints on the timing and extent of this and other pyroclastic flow deposits of the North Mono eruption.

The sides and the lobate terminus of the west flow deposit are quite distinct (Figure 12). Debris constituting this deposit was ejected from a vent or vents now buried under Northern Coulee and covers an area of about 6.5 km^2. Numerous ridges, up to several meters high and more than 100 m long, are elongate parallel to the sides of the flow unit. The deposit is massive, compact, white to pale pink, and very poorly sorted. Near its terminus it is only a meter or so thick, but on its eastern edge it is probably at least 30 m thick, judging from its topographic expression. Its volume is about 0.05 km^3.

The west flow deposit clearly overlies air fall bed 1 and several younger, well-preserved pumiceous air fall beds at "jg" (Figure 12). In a nearby pit the flow consists of at least two flows, each overlain by a portion of the

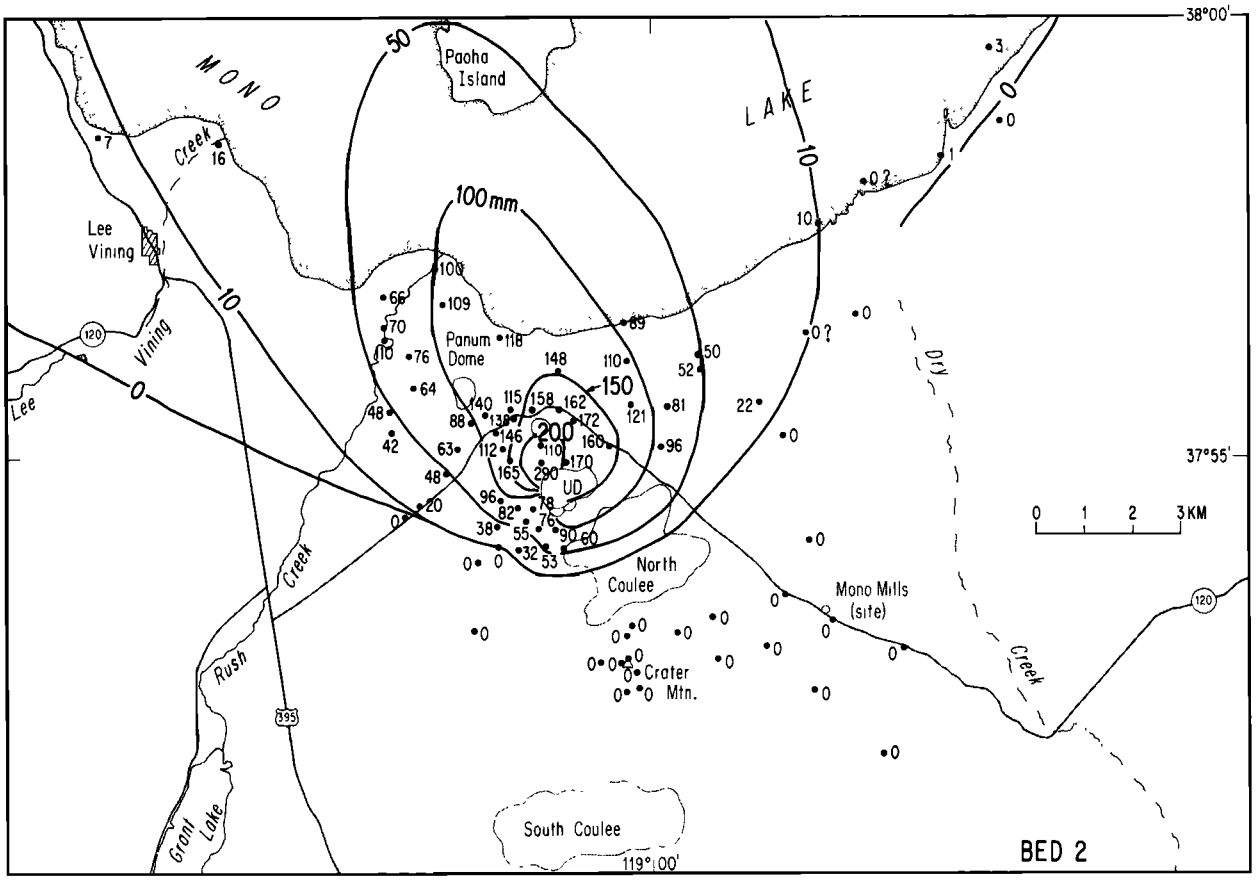

Fig. 7. Isopach map of the proximal portion of bed 2 indicates winds toward the north-northwest during the eruption and a source vent now buried beneath Upper Dome (UD).

planar-bedded GGB. Therefore at least the upper parts of the west flow deposits are correlatable with flow deposits intercalated with the GGB northeast, north, and south of Northern Coulee. Planar-laminated gray glassy ash more than 2 m thick overlies the flow near "je." At site "gg" the flow overlies two thin, well-preserved air fall beds of white pumice and has a thin, highly bioturbated mantle of GGB.

On the steeply northeast sloping, forested plain southeast of Northern Coulee, the air fall beds are locally mantled by cross-laminated ash beds. Leeward slip faces dip N25°E, parallel to nearby 1- to 2-m-high ridges. These beds and longitudinal dunes must represent grain-by-grain deposition of a saltating bed load at the base of a highly inflated cloud moving rapidly eastward down the flanks of the Mono Craters. In one exposure, these beds are overlain by gray glassy air fall beds (GGB).

Domes and Coulees

Five separate domes and coulees and four tephra rings and ridges are the youngest products of the North Mono eruption. From north to south the domes and coulees are Panum Dome, Cratered Dome, Upper Dome, an unnamed satellite of Upper Dome, and Northern Coulee (Figure 10b). The barrenness of these rugged, craggy domes and coulees testifies to their relative youthfulness because these extrusions would bear a thick mantle of the North Mono tephra if they had been extruded prior to the pyroclastic phases of the eruption.

Northern Coulee, the southernmost and largest of these aphyric rhyolite lava flows, was named by Russell [1889]. Because it has been mapped in detail recently by Kelleher [1986], we will not discuss it in detail here. Several aspects of its geometry and history, however, should be mentioned.

Northern Coulee is the largest single unit of the North Mono eruption: its volume is 0.4 km^3, well over half the total volume of the eruption. It is a composite flow which originated from a northwest-trending fissure or alignment of vents. Two separate stubby flows moved westward and southwestward from this source fissure; two other lobes, each consisting of two or more coalescing flows, moved northeastward from the source region.

Locally, Northern Coulee is mantled by thick accumulations of ashy to blocky tephra that bear a striking textural resemblance to the GGB. Furthermore, a curiously solitary northwest-striking ridge, also composed of ashy to blocky gray glassy tephra, lies on the western edge of Northern Coulee. The two westward and southwestward lobes of the coulee appear to have flowed around the ridge. This 330-m-high symmetrical edifice must be the result of a late-stage, low-altitude fountaining of pyroclastic debris from the source fissure. And

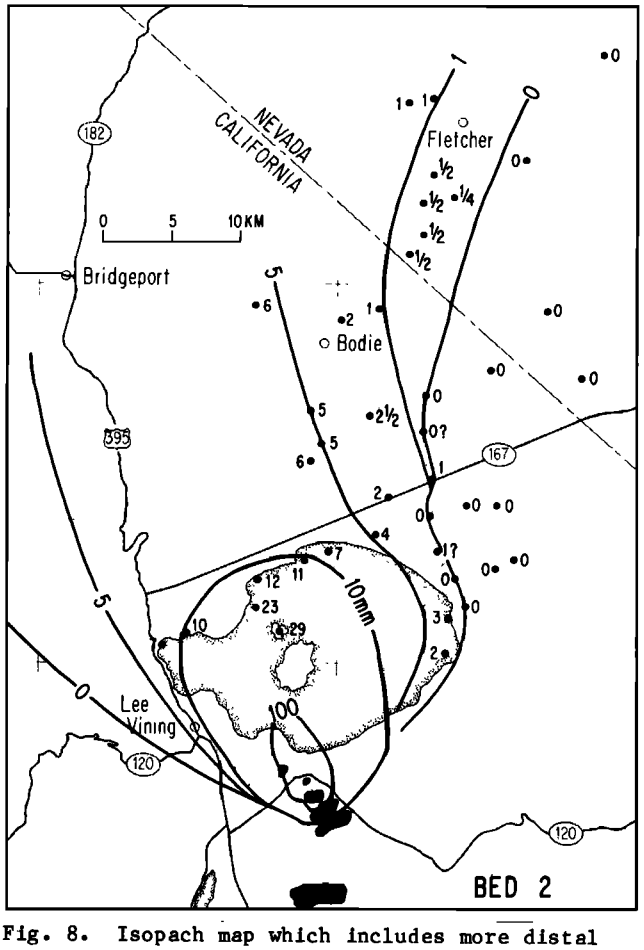

Fig. 8. Isopach map which includes more distal portion of bed 2 indicates winds toward the north-northwest at lower altitudes and, perhaps, a north-northeasterly flow at higher altitudes.

yet, if this is so, the tephra ridge would be expected to have a matching ridge on the opposite (northeastern) side of the source fissure. This twin may be missing because it was disarticulated and rafted away to the northeast atop the northeastern lobes of the coulee. The thick, isolated accumulations of tephra on these lobes may be rafted fragments of this former tephra ridge. Alternatively, strong winds blowing out of the northeast at the time of the eruption might have prevented formation of a tephra ridge northeast of the vent.

Upper Dome is the second most voluminous lava flow of the North Mono eruption and was given its name by Wood [1977a], who noted its position atop Northwest Coulee, a larger tephra-mantled flow. Upper Dome has also been mapped in detail by Kelleher [1986] and will not be discussed in detail here. We note, however, that the source of this dome is near its western edge and that the eastern part of the flow moved down the steep eastern flank of the older subjacent coulee.

A very small dome and a tephra ring, both subsidiary to Upper Dome, are present on its southern flank (Figure 10b). The subsidiary or satellite dome fills the bottom of a partially preserved crater, and the tephra ring lies east of the small dome. The northern half of the tephra ring is clearly overridden by and hence is older than Upper Dome. The satellite dome also appears to be overridden by and hence older than Upper Dome.

Cratered Dome is a small, isolated dome immediately south of Highway 120 which was mapped in detail by Smith [1973]. Cratered Dome has no tephra ring, and no pyroclastic fall or flow beds appear to have originated from the vent from which it was extruded.

History of Panum Crater

Panum Crater has long been a particularly attractive geological feature of the Mono Basin. One hundred years ago, I. C. Russell and his talented topographer W. T. Johnson first described and explained the pristine dome that resides within the crater and the imposing ring of tephra that surrounds it [Russell, 1889].

The dome and tephra ring are, however, the products of the least explosive phases of the eruption of Panum Crater. Widely dispersed pyroclastic flow and surge deposits that blanket the plain surrounding the crater record earlier and more violent phases of its eruption.

The eruptive history of Panum Crater is particularly well understood because quarrying operations adjacent to the vent on the southeast and stream erosion to the west have exposed many of its deposits. Furthermore, the vent is well removed from other sources of North Mono tephra, so its deposits are not complexly intercalated with those of the other vents. Because it is so well understood, we have chosen to discuss the entire evolution of Panum Crater together in this section. (We use "Panum Crater" when referring to the orifice through which the various deposits were evacuated, and we use "Panum Dome" only in

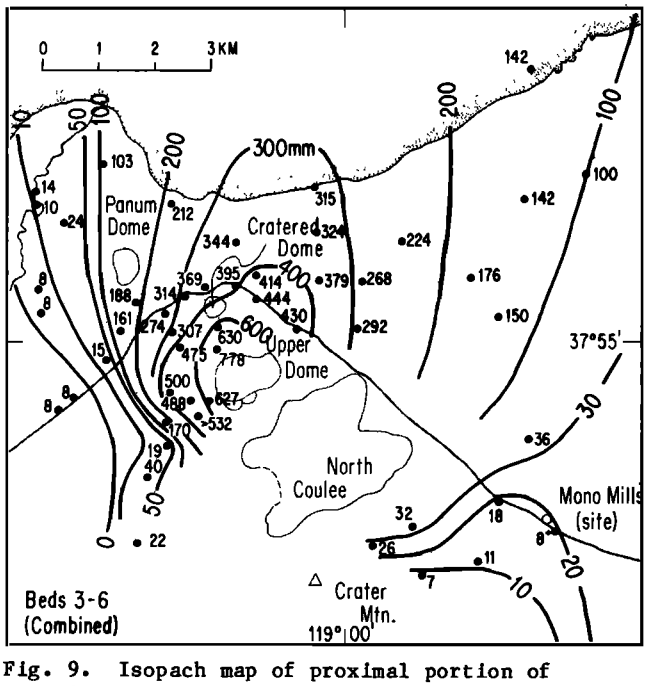

Fig. 9. Isopach map of proximal portion of beds 3-6. Map of distal portion available on microfiche, Figure A2.

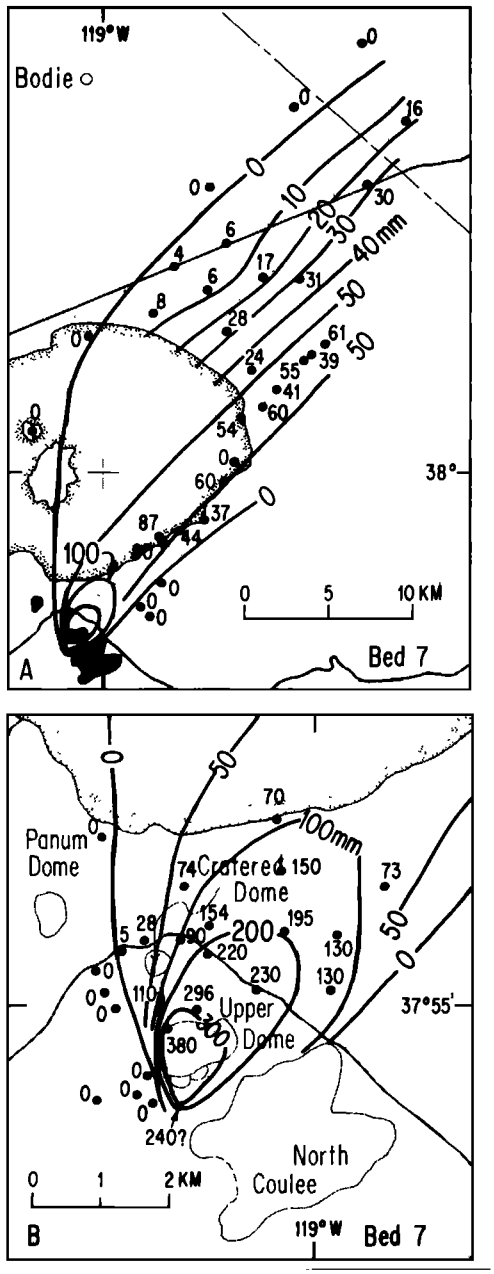

Fig. 10. Isopach maps of bed 7 show northeasterly trend of dispersal axis. (a) Far-field data show extraordinary asymmetry and elongation of isopach contours. (b) Near-field data show that a vent near or under Upper Dome was the source of bed 7.

reference to the rhyolitic plug that now resides within the crater.)

Throat-clearing breccia. Figure 13 is a generalized, composite columnar section of the products of Panum Crater. At the base of the section are found all the North Mono air fall beds, which had fallen prior to excavation of the crater. None of the major air fall beds of the North Mono tephra originated from Panum Crater. In an exposure about 1 km northeast of Panum, beds 1, 2, and 3 and the GGB unmistakably underlie the oldest surge and flow deposits traceable to Panum Crater. This confirms that the air fall beds, including all the GGB that fell at this location, antedate the creation of Panum Crater. Activity at Panum, therefore, occurred very late in the North Mono eruption.

The first evidence of activity at Panum is a massive, unsorted, heterogeneous breccia that overlies the North Mono air fall beds up to 650 m from Panum Crater. This unit, exposed best in a quarry southeast of Panum Dome, is clear evidence for the rapid, violent creation of a crater in the fluvial and lacustrine sediments underlying the Mono Craters. About 10-20% of the volume of this heterogeneous bed are angular lapilli and small blocks of laminated silt and rounded Sierran gravel, torn from late Pleistocene lacustrine and fluvial beds in the shallow subsurface. The ashy matrix of the breccia is composed of Sierran and young silicic volcanic materials.

Calculation of the volume of the ashy breccia yields a crude estimate of the size of the crater left by its removal. If one assumes a radially decreasing thickness for the bed that is consistent with measurements in several pits and assumes a conical explosion crater with a 440-m diameter (equal to the east-west diameter of the crater at the level of the surrounding plain), the throat-clearing breccia has a volume of 2.6-4.3 x 10^6 m^3. This volume would fill a 440-m-wide conical crater 50-85 m deep.

This calculated depth is perfectly consistent with the observed lack of angular fragments of Bishop Tuff in the breccia. On the basis of outcrops several kilometers to the south [Kistler, 1966] and a well drilled about 2 km to the northeast [Axtell, 1972], the top of the Bishop Tuff lies about 220 m beneath the surface of the plain into which Panum Crater was excavated. Thus the Bishop Tuff lies well below the calculated depth of the crater.

Perhaps the most plausible explanation for the creation of the throat-clearing breccia is that the rising magma, upon breaching the Bishop Tuff, caused the interstitial water in the overlying gravels and sands of the Rush Creek delta to flash to steam. Similar deposits studied by other workers at other localities have been ascribed to the violent and sudden interaction of magma and external water [Fisher and Schmincke, 1984, pp. 257-260; Wohletz and Sheridan, 1983].

Panum Dune flow deposit. The stratigraphic record reveals that the initial excavation of Panum Crater was followed by eruption of a pyroclastic flow. That flow deposited a massive bed composed principally of subrounded, white to silvery-gray, lineated pumiceous ash and lapilli (Figure 13). Sparse, rounded Sierran granitic clasts indicate that minor entrainment of fluvial gravels occurred at shallow depths in the volcanic conduit during the eruption of this unit. This pumice flow appears to have left coarse debris in all quadrants surrounding Panum Crater, but we consider correlation of the bed between excavations to be tentative.

In the quadrant southwest of the crater the pumice flow left an intriguing dune field first pointed out to us by R. Bailey. Figure 12 shows the crestal traces of some of the larger dunes. These dunes are commonly a few tens of meters apart, 0.5-1.0 m in height, and rarely more than

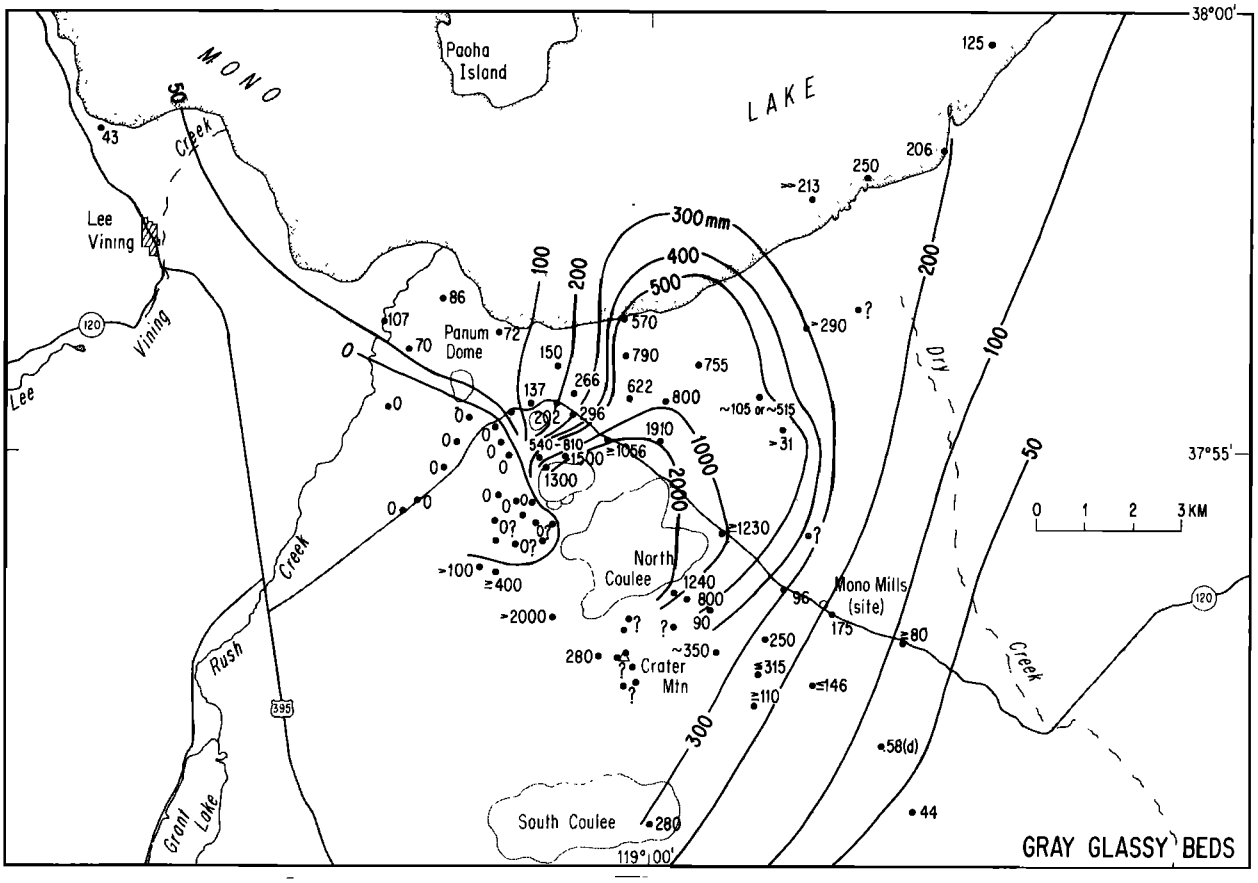

Fig. 11. Isopach map of proximal gray glassy beds indicates multiple sources between Upper Dome and Northern Coulee. Most of this tephra was blown north and east of the source(s), but a significant fraction was blown toward the south and west. Map of distal gray glassy beds is available on microfiche, Figure A3.

300 m long. Excavations within the dune field revealed them to be composed of the subangular white lapilli and fine blocks. Charred twigs are common within the dune bed. The pyroclasts must have been the bed load of a hot, radially expanding cloud.

The dune crests appear to be roughly concentric about a location 1000 m south of Panum Crater. This suggests a source well south of Panum Crater, closer, in fact, to an older crater southeast of Panum. This source is rendered impossible, however, by the observation that the North Mono air fall beds that underlie the dune bed overlie the rhyolite dome that fills the older crater. Hence the older crater antedates the North Mono eruption. Although Panum Crater was certainly the source for the dune flow deposit, the flow field responsible for it remains a puzzle.

Panum pyroclastic surge beds. Overlying the Panum Dune flow is a series of pyroclastic surge beds intercalated with minor air fall beds. Thickest exposed sections of these beds (1-2 m) are in quarry exposures southeast of Panum. Surge beds there consist of well-laminated planar- and cross-bedded yellowish-brown ash beds. Paleocurrent directions determined from sets of climbing ripples with amplitudes of about 10 cm and wavelengths of 1-1.5 m are away from Panum Crater. Fine-grained, cross-laminated volcanic deposits such as these have been recognized at many localities where magma and external groundwater or open bodies of water have interacted violently (for example, see Moore et al. [1966]; Wohletz and Sheridan [1983]). At least four horizons within these surge beds are deformed by small, angular block bombs of dense, nonpumiceous rhyolite. These bombs may also represent explosions produced by interaction of magma and groundwater within Panum Crater.

Panum block-and-ash flow deposit. In the quadrant north and west of Panum Crater, a very coarse block breccia overlies the surge and flow beds just described. This deposit was first recognized by Wood [1977b, p. 94], who called it a "block avalanche." Because this term implies an origin by gravitational collapse of an exogenous dome, we have chosen to refer to it more descriptively as the Panum block-and-ash flow deposit (Figures 12 and 13).

The Panum block-and-ash flow deposit is a fan-shaped body composed of aphyric ash, lapilli, and blocks with stony to pumiceous textures and rhyolitic composition. Both coarseness and sorting decrease northwestward, away from the source. Maximum exposed thickness is about 15 m, distal thicknesses are of the order of a meter, and proximal thickness could well be a few tens of meters. This pyroclastic fan covers an area of about 3.5 km^2 and has a dense-rock-equivalent volume of about 0.013 km^3.

The deposit is constrained on the southwest

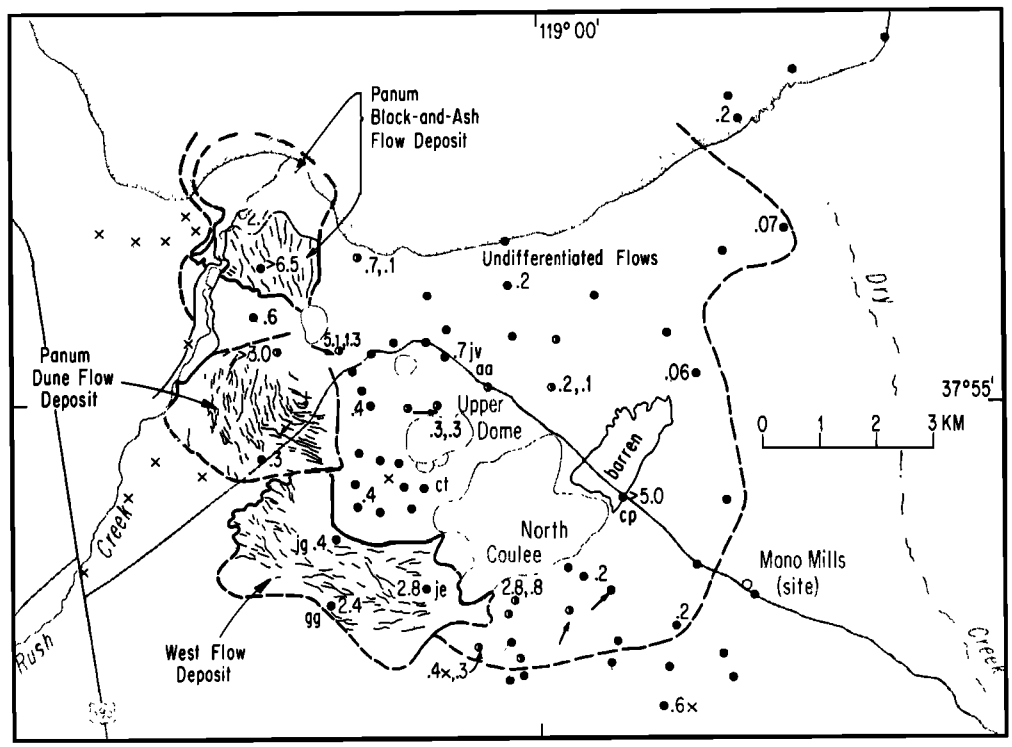

Fig. 12. Map of known extent of pyroclastic flow and surge deposits. Geomorphically distinct flows are labeled "west flow," "Panum Dune flow," and "Panum block-and-ash flow". Dune flow and block-and-ash flow have been eroded along Rush Creek, and the northern half of the block-and-ash flow has been eroded and buried during recent high stands of Mono Lake. Dots indicate natural or man-made outcrops in which unambiguous flow or surge deposits are exposed. Crosses denote outcrops in which bioturbation is so great that flow deposits cannot be identified with certainty. Numerals alongside dots indicate total thickness (in meters) of flow and surge deposits. Arrows indicate paleocurrent directions. A more complete display of the data from which this figure was constructed is available on microfiche, Figures A5 and A6.

and east between two slopes, which Wood [1977a] speculated are fault scarps. Prominent ridges and large blocks ornament the surface of the Panum block-and-ash flow deposit. Like the ridges on the west flow deposit described above, these ridges converge uphill toward the inferred source, which in this case is Panum Crater. The terminus of the flow is preserved on its southwestern end against the western wall of the Rush Creek gorge (Figure 12). The deposit there is about a meter thick and has an irregular, geomorphically visible terminus. The flow deposit clearly blocked Rush Creek upon emplacement, but the creek has subsequently eroded a new channel completely through the deposit and is currently flowing within a fraction of a meter of its former elevation. At elevations below the level of the ~200-year-old high stand of Mono Lake (about 6456 feet [1968 m] [Stine, 1984]), the surface of the deposit has been reworked by littoral processes and buried by lacustrine sediment; hence the margins of the deposits are ill-defined below 6456 feet (1968 m).

In exposures about 1.5 km from Panum Crater, well above lake level, the deposit is more than 6.5 m thick and consists of well-sorted, partially agglutinated lapilli and blocks. About 90% of the pyroclasts are angular fragments of nonpumiceous to weakly pumiceous gray glass. The surfaces of these stony-looking pyroclasts commonly display thin and patchy terra cotta stains which probably represent precipitation of iron oxides after emplacement. Internal fractures within these blocks are rare and probably formed in situ by thermal contraction. Most of the blocks display white powdery spots on their surfaces, which we interpret to be the result of impacts with other clasts during transport. These marks, the lack of bread-crust textures, and the extreme angularity of the stony clasts indicate that they behaved brittlely during transport. Nevertheless, Salyards [1986] reports emplacement temperatures greater than 600°C for these blocks, based upon paleomagnetic analysis.

About 10% of the volume of the deposit in these outcrops are small blocks of black to light gray, highly vesiculated, foliated pumice with pronounced bread-crusted surfaces. Commonly, these clasts have lumpy exteriors and partially enfold smaller pieces of the angular, stony rhyolite. The angular rocks clearly pressed into the bread-crusted material while it was still hot and ductile. This interpretation is supported by the high temperature of emplacement indicated by Salyards's [1986] paleomagnetic results, by pinkish casts in the uppermost portions of the

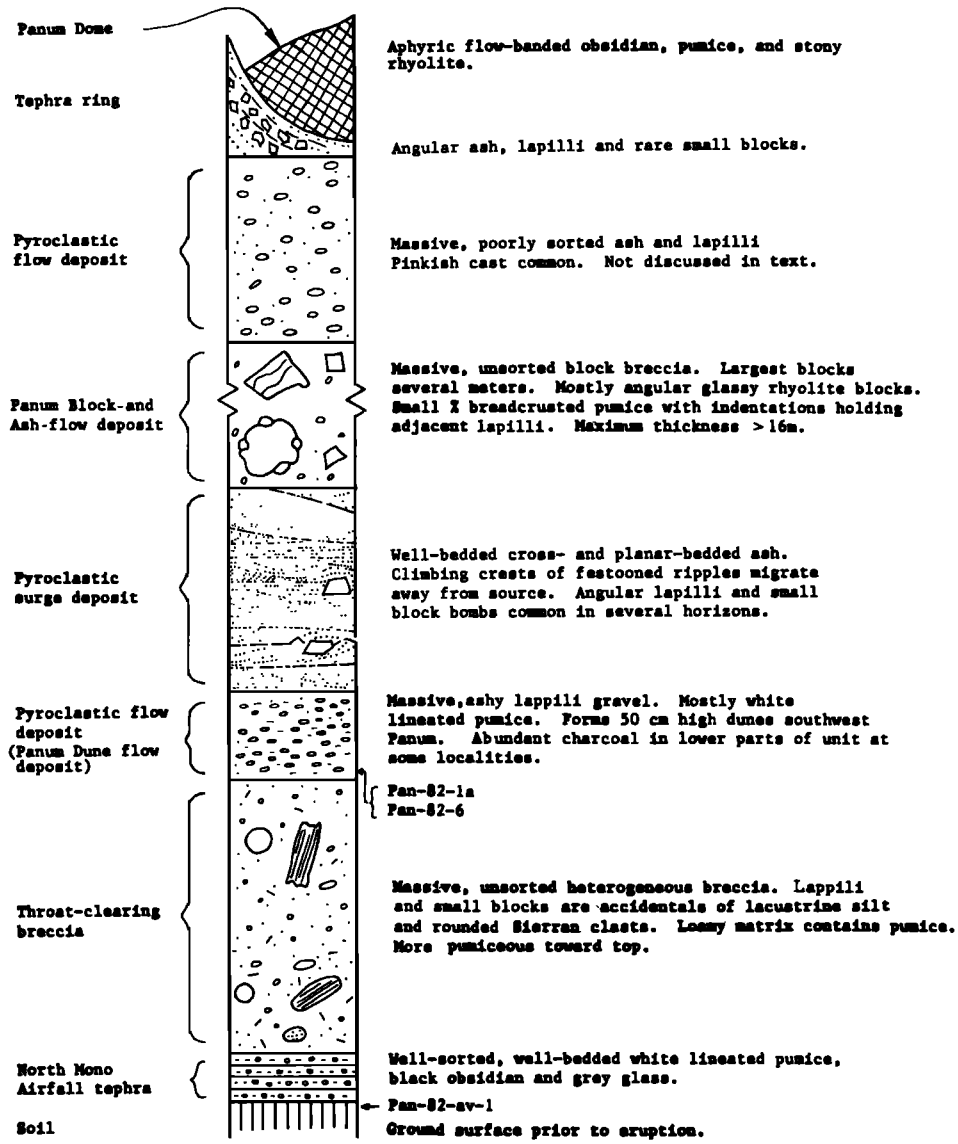

Fig. 13. Generalized columnar section of deposits of the North Mono eruption in the vicinity of Panum Crater. Also shown are stratigraphic locations of the radiocarbon samples listed in Table 1.

deposit, and by the presence of degassing pipes in exposures of the deposit on the banks of Rush Creek.

The presence of two distinct populations of pyroclasts, one with textures indicating brittle behavior during flow and the other with textures indicative of ductile behavior during flow, constrains interpretation of the origin of the deposit. The commonly ascribed origins for block-and-ash flows, collapse of a partially molten exogenous dome or explosion of a shallow cryptodome (that is, an intrusive dome lying at a shallow depth) [Williams and McBirney, 1979, pp. 152-153], may well be the best explanations for this deposit. The angular and stony textures of most of the blocks are similar to the dominant textures found in the domes and lava flows of the North Mono eruption and are very much unlike the subrounded, lineated, pumiceous textures found in other pyroclastic flows of the eruption. The estimated dense-rock-equivalent volume of the deposit, 0.013 km^3, approximately equals that of Panum Dome (0.012 km^3), suggesting that if the flow originated by collapse of an exogenous dome, the dome would have been about the same size as Panum Dome. Observations of the June 12, 1980, eruption of Mount St. Helens [Moore et al., 1981, p. 542] and elsewhere [Williams and McBirney, 1979, p. 153] suggest that block-and-ash flows can also result from the explosive disintegration of a cryptodome.

Emplacement of the Panum block-and-ash flow upon the sandy, pebbly sediments of the Rush Creek delta resulted in spectacular deformation that merits separate discussion. Below an elevation of about 6430 ft (1960 m), most creekbank exposures of the base of the block-and-ash flow deposit display one or more of the following features: large rotated blocks of substrate widely separated by fissures filled with the block-and-ash flow debris and resting on a decollement; substrate and North Mono air fall

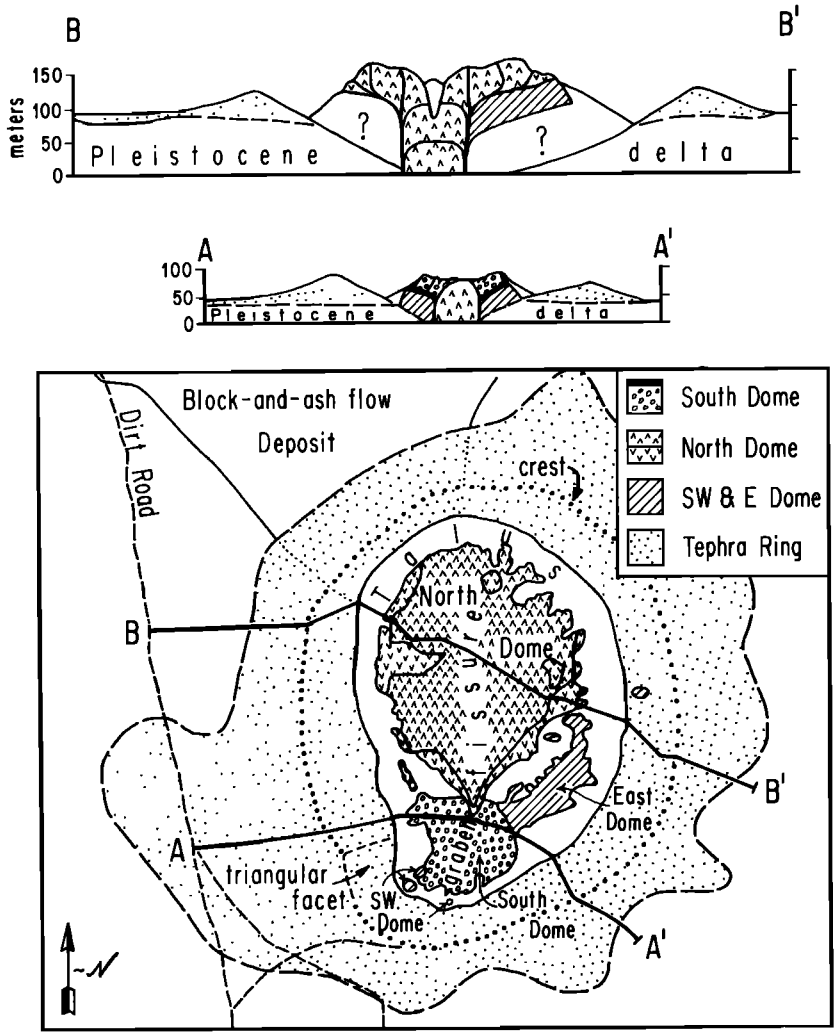

Fig. 14. Generalized map and cross sections of Panum Dome. Base is U.S. Forest Service aerial photograph.

tephra distorted into faulted, tight, overturned folds commonly resting on a decollement and overlain by the flow deposit; small, disarticulated blocks of sandy substrate floating in a matrix of homogenized components of the block-and-ash flow and substrate, overlain by the flow deposit and resting upon a sharp decollement. Apparently, these formed by sudden loading and resultant liquefaction of water-saturated fluvial sands. However, an analysis of the mechanism of deformation is beyond the scope of this study.

Panum tephra ring. The last major pyroclastic deposit to exit Panum Crater is the tephra ring that circumscribes the crater and rises about 70 m above the Pleistocene delta plain of Rush Creek (dot pattern in Figure 14). Ash, lapilli, and small blocks of this deposit are restricted to an elliptical region that extends up to 700 m from the center of the crater. Accidentals are sparse but conspicuous and include rounded Sierran plutonic and metasedimentary rocks eroded from underlying gravels of the Rush Creek delta. The ring mantles the delta plain on the west; an older dome and crater on the south and southeast; blocky, hummocky debris of unknown origin on the east and northeast; and the surface of the Panum block-and-ash flow deposit on the north. The outward facing slope of the tephra ring is parallel to bedding and is a constructional surface built up by aggradation of pyroclasts falling upon it. The inward facing slope of the tephra ring cuts across outward sloping bedding in many places and thus appears to be a destructional surface, formed either by removal of tephra by pyroclasts exiting the crater at low angles or by slumping of tephra back into the crater. In either case, widening of the crater during formation of the tephra ring is indicated.

The crest of the tephra ring is unusually low both on the north and the south. To some degree this must be a consequence of eruption from an elongate vent. Uniform mass rates of eruption from a fissure will lead to more debris accumulating on the flanks of the fissure than on the tips because the region around the fissure tip receives material from a smaller portion of the vent. On the north, however, the rim is also low because the tephra mantled the preexistant notch through which the block-and-ash flow deposit exited Panum Crater. On the south, the

rim was lowered by an explosion that must have originated beneath what is now the southern part of Panum Dome. Evidence of this small explosion includes the triangular facet on the southwest side of the tephra ring (Figure 14) as well as other geomorphologic features. This small explosion probably antedated the emplacement of most of Panum Dome, since the dome does not appear to have suffered an explosion.

Panum Dome. Panum Dome is the final erupted product of Panum Crater. Actually, it consists of two exogenous domes and two smaller dome fragments, all of which are structurally and texturally distinct. Only the primary features of this composite dome are illustrated in Figure 14 and discussed here.

The largest and youngest dome, North Dome, occupies the northern two thirds of the edifice. It consists of a light gray, flow-banded stony rhyolite surrounded by a collar of bread-crusted, light gray pumiceous rhyolite and has a strong bilateral symmetry about a north-south fissure. Flow bands, radially widening fractures, and other structural data indicate that the dome issued from a north-south fissure somewhat shorter than the north-south diameter of the dome. Most of the lava issued from the central portion of the fissure, with the result that the dome is elliptical in plan. The steeply inward dipping surfaces of the eastern and western half of North Dome (Figure 14, cross section B) appear to have exited the vent juxtaposed in a vertical or near-vertical position and then to have tilted outward and away from each other.

South Dome lies south of and is bisected by the southern extremity of North Dome (Figure 14). This smaller dome is cored by gray and black banded rhyolite and obsidian and has a 10-m-thick carapace of foliated pumice topped by a discontinuous shell of massive black obsidian up to a meter thick. South Dome is bilaterally symmetrical about a north-south graben. This graben formed by brittle extension of South Dome during the shallow intrusion of unexposed underlying magma, probably the North Dome diapir (see Figure 14, cross section A).

Southwest and East domes are fragments of a dome or domes emplaced prior to extrusion of South Dome and North Dome. The Southwest Dome fragment consists of two large blocks of white stony rhyolite and numerous smaller (unmapped) blocks on the western flank of South Dome. Some of these blocks rest immediately above or are floating within the obsidian carapace of South Dome, an indication that the Southwest Dome fragments were pushed out of the way by South Dome.

East Dome consists of a highly fractured stony to very pumiceous rhyolite. The fractures may well have formed during intrusion of North Dome. This dome fragment has a thin mantle of tephra locally.

Source Region

From the maps of the several pyroclastic fall and flow deposits presented above, the multiple-source nature of this eruption is already quite apparent. In this section we interpret those maps along with geomorphologic and structural evidence in order to present a clearer picture of the source vents and the sequence of their eruption.

Sources of the Various Deposits

The vents from which the North Mono tephra and related lava were erupted are at least 10 in number. These separate craters and source regions are displayed in plan view in Figure 15a. Several of the vents (that is, those numbered 4-8, and southernmost 9) are still visible craters, unfilled or only partially filled with domes or coulees. The actual shapes and sizes of those vents now completely buried beneath the domes and coulees, while not directly observable, can be inferred from the configuration of the domes and coulees as well as from the isopach maps of the air fall beds. The axial north-south fissure and internal structure of Panum Dome and Panum's elongate tephra ring, for example, indicate that source 1 was elongate north to south, at least in the late stages of its eruption. The north-south crest of Northern Coulee also requires an elongate source or alignment of sources like that depicted as source 9.

Figures 15b-15h show the source vents or vent regions for beds 1-7, as well as those for the gray glassy beds, the pyroclastic flows, and the domes and coulees. These are based upon the isopach maps and related data presented and discussed above. Judging from its isopach map (Figure 5), bed 1 pyroclasts were expelled from sources now buried beneath Northern Coulee, in the vicinity of the long linear source labeled "9" (Figure 15b). Source 10, which is the site of a late-stage eruption of black pumiceous lava through the main body of Northern Coulee, could also be one of the sources. Source 8, however, is not a plausible contributor to bed 1. In the northwestern wall of this crater, beds 1, 2, and, probably, 3 rest directly upon a flat-lying, weathered, substantially older tephra and are buried by about 12 m of blocky debris that was thrown up onto the rim of the crater when the crater was excavated. Thus crater 8 came into being after the deposition of beds 1 and 2 and probably beds 3-6.

The isopach map of bed 1 is not detailed enough to reveal the fine structure of source 9. That source could consist of two or more circular craters or a solitary fissure. In either case, the source must be elongate north to south and must extend 1.5-2 km in order to account for the shape of the 300-, 400-, and 500-mm thickness contours shown in Figure 5.

The isopach map of bed 2 (Figure 7) indicates that bed 2 pyroclasts were expelled from source 3, now buried beneath the western portion of Upper Dome (Figure 15c). Sources 4 and 5 are plausible additional vents for bed 2.

On the basis of the isopach map of Figure 9, beds 3-6 were evacuated from vents as far north as source 3 and as far south as source 9 (Figure 15d). Bed 3 clearly was evacuated from source 3 and at least one or more sources beneath Northern Coulee. Available data for beds 4-6 are too sparse to be conclusive but do suggest that some of these beds also resulted from simultaneous eruption of southern and northern

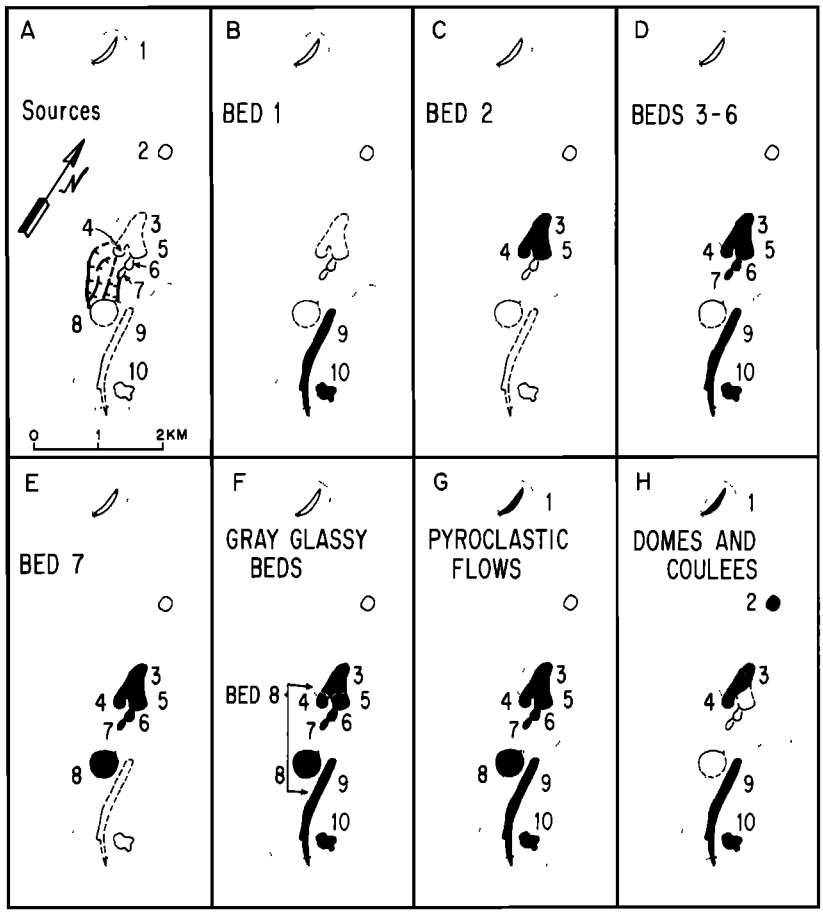

Fig. 15. Source vents for the North Mono tephra and associated lava. Dots outline Panum Dome, Upper Dome, and Northern Coulee. Solid lines indicate geomorphologically and structurally mappable vents. Dashed lines indicate inferred geometry of vents now buried beneath Upper Dome and Northern Coulee. Heavy lines in Figure 15a represent traces of faults believed to be related to the North Mono eruption. Vents in solid black are plausible sources for units indicated in each block.

sources. Sources 4-7 are plausible, but not confirmed, sources of beds 3-6.

The fact that bed 3-6 materials exited from more than one vent allows the possibility that the odd facies variations in beds 3-6, described in the preceding section, are the result of simultaneous eruption from more than one vent. The more northerly vent or vents might have undergone several discrete pulses of eruption, leading to several distinct beds, whereas the more southerly vents might have experienced a more nearly continuous eruption of pyroclasts.

Isopachs of bed 7 (Figure 10) clearly indicate that source 3 was a vent for bed 7 and that sources 1, 2, 9, and 10 were not (Figure 15e). Sources 4, 5, 6, 7, and, perhaps, 8 are also plausible contributors.

The GGB are thickest and coarsest in the region surrounding Northern Coulee and Upper Dome (Figure 11). This suggests multiple sources for the beds. Other stratigraphic observations also support this conclusion. Pits just north of Upper Dome display growth faults, cross-bedded pyroclastic surge beds, and erosional scours within the gray glassy unit, features that indicate proximity to source.

The initial source of the gray glassy unit is a vent somewhere between Upper Dome and Northern Coulee. This is shown by the isopach map of the basal GGB, bed 8 (Figure A4, available on microfiche[1]). This bed is a distinctive white tephra that constitutes the base of the GGB northeast of Upper Dome. The isopach pattern points to one or more vents between Upper Dome and Northern Coulee and appears to exclude source vents under Upper Dome and the southern half of Northern Coulee.

The sources of several pyroclastic flow deposits are well constrained. The geometries of the throat-clearing breccia, the Panum block-and-ash flow deposit, and the Panum Dune flow require eruption from Panum Crater (source 1). For the same reason, the undifferentiated pyroclastic flow unit atop these beds in the vicinity of Panum Crater also appears to have Panum Crater as its source. The source or sources of the west flow deposit are also well

[1]Supplemental figures are available with entire article on microfiche. Order from American Geophysical Union, 2000 Florida Avenue, N.W., Washington, DC 20009. Document B86-006; $2.50. Payment must accompany order.

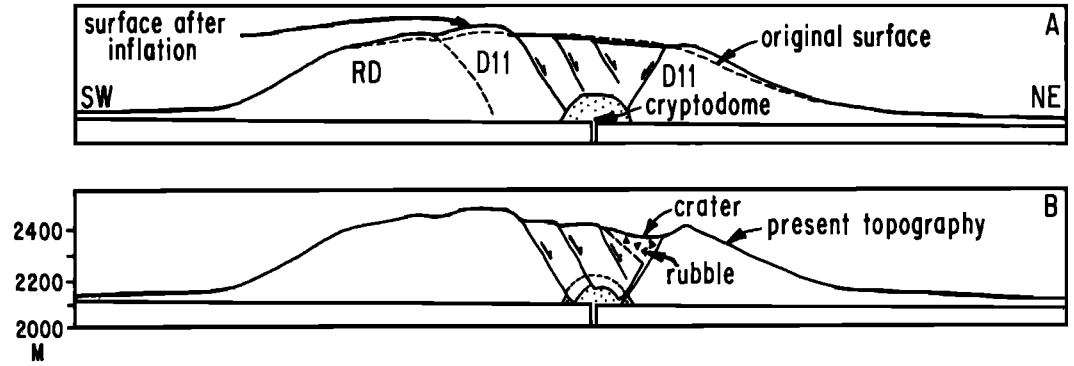

Fig. 16. Cross section across graben associated with the North Mono eruption. (a) Hypothetical inflation of Mono Craters edifice and normal faulting caused by the intrusion of cryptodome at base of the volcanic pile. (b) Present topography resulting from deflation of the hypothetical cryptodome by eruptive evacuation.

constrained by the deposit's geometry. It must have originated from one or more sources beneath Northern Coulee (that is, vents 8, 9, and/or 10).

The sources of the minor ash flow deposits between beds 6 and 7 are constrained by their thickness and distribution to sources in the vicinity of Upper Dome and Northern Coulee (that is, sources 3-10). The thick pyroclastic flows found on the plains north and east of Upper Dome and Northern Coulee also are loosely constrained to these source vents. More detailed work might enable better differentiation of these flows and could lead to more specific identification of sources.

Graben

Another interesting structure within the source region is a 600-m-wide graben which trends northwestward between Northern Coulee and Upper Dome. The normal faults that bound this graben are shown on Figure 15a. These faults exhibit dip slippage of several tens of meters and lengths of up to 700 m. The walls of craters 4 and 8 are unbroken by the faults, so one can conclude that all major slip on the faults preceded the opening of at least these two vents. Exposures on the rims of these two craters show that they were excavated some time after the eruption of bed 1 and 2 pyroclasts. However, we do not know whether the graben faults formed before or after deposition of beds 1 and 2.

The graben surely formed in response to an extensional stress field in which the least principal stress was oriented approximately perpendicular to the strike of the graben, that is, northeast-southwest. The dip of the faults is unknown, but if the faults dip 60°, dip-slip on them accommodated about 60 m of northeast-southwest extension. Steeper faults would, of course, require less extension.

The fact that this extension occurs across a width of only 600 m indicates that its causative agent was operating at very shallow depths. One plausible mechanism for the formation of the graben would be inflation of an elongate north-south trending sill or cryptodome within the edifice of the volcanic chain. This might well produce an arching of the superjacent rocks and formation of a graben along its crest, as illustrated in Figure 16a. Evacuation of all or part of the cryptodome during eruption could be expected to result in additional slip on the graben faults (Figure 16b). A cryptodome with a volume of about 0.1 km^3 could produce the observed fault displacements in the manner shown by the figures.

An alternative hypothesis is that the graben resulted from intrusion of a wide north-south striking dike into the edifice of the Mono Craters. Pollard et al. [1984] have shown that a pair of parallel tensile cracks can be produced by a magma-filled dike intruding the shallow subsurface. Their mathematical model indicates that as the dike rises toward the surface, zones of tensile stress develop above and off to the sides of the dike. When these tensional regions intersect the ground surface, tensile ground cracks develop parallel to the dike if the tensile stress exceeds the tensile strength of the rock. They also find that the distance between these cracks is 2-3 times the depth of the top of the dike. In this case, the spacing of the outermost faults, about 600 m, would indicate that tensile failure began when the dike had risen to within 200-300 m of the surface, well within the volcanic edifice. The lack of faults in the central 200 m of the graben may indicate that the dike rose no closer to the ground surface than 70-100 m.

Pollard et al.'s model explains the occurrence of tensile fractures above the dike top but does not explain the large amount of throw on the graben faults. However, once tensile cracks form in the manner explained by them, widening of the intruded dike by injection of additional magma would result in substantial slippage on normal faults overhead. In this case, in which total dip-slip across the faults is about 100 m, a dike width of about 60-20 m would be necessary for 60°- to 80°-dipping faults. These values are substantially greater than the widths of most silicic dikes reported in the literature [e.g., Lipman, 1984]. However, the dike or pipe recently encountered beneath one of the Inyo Domes at a depth of several hundred meters was found to be about 70 m wide [Eichelberger et al., 1985]. If in fact the graben did form by extension of the rocks overlying a wide dike, the

timing of graben formation relative to the various eruptive pulses of the North Mono eruption is critical to understanding the nature of the eruption.

Dike Intrusion During the North Mono Eruption and During Other Multiple-Vent Silicic Eruptions

Several pieces of evidence described above lead us to conclude that the North Mono eruption resulted from shallow intrusion of a rhyolitic dike or dikes. These data are (1) the elongate nature of the source of bed 1 and Northern Coulee, (2) the axial fissure of Panum Dome, (3) the rough alignment and near contemporaneity of all 10 source vents, (4) the compositional uniformity of the material that was discharged from these vents, and (5) the 700-m-long graben between Northern Coulee and Upper Dome. Individual sources (1 and 9 in Figure 15) are elongate in a direction about 30° more easterly than the general alignment of the sources. Furthermore, sources 3 and 4 and sources 5, 6, and 7, form northeastward trends. This en echelon geometry is very similar to that of the Inyo Domes, which Fink [1985] interprets as indicating a near-surface clockwise rotation and segmentation of a dike that is contiguous in the subsurface.

The contemporaneous or nearly contemporaneous eruption of the North Mono Tephra and lava flows from a 6-km-long source region is not without analogues. Fink and Pollard [1983] examined an alignment of fissures, phreatic explosion craters, and rhyolitic domes associated with a Plinian eruption in northern California and inferred intrusion of a dike into the shallow subsurface. Scott [1983] reports an alignment of young silicic domes in southern Oregon that appear to have erupted contemporaneously. Miller [1985] concludes that the 11-km-long alignment of the youngest Inyo Domes, related explosion craters and fissures, just south of the Mono Craters, resulted from a single eruptive episode a little more than 600 years ago and, with Fink [1985], interprets this alignment as evidence for shallow intrusion and venting of a silicic dike.

The historical eruption of Krakatau in 1883 may also be analogous to the North Mono eruption in that multiple, aligned vents were active during its early stages. Eyewitness accounts assembled by Simkin and Fiske [1983, pp. 58-68] document the progressive opening of three major and at least 11 lesser vents in the 3 months prior to the caldera-forming paroxysm. These vents were located along a 4.5-km line that crossed the center of the future 10-km-wide caldera and were observed in simultaneous eruption 2 weeks before the climactic eruption. Simultaneous eruption from four separate localities was also observed during the previous, smaller eruption of Krakatau in 1681 [Simpkin and Fiske, 1983, p. 286].

From these several examples one can conclude that the eruption of silicic magma from aligned vents is not uncommon. In many or perhaps all of these cases, these alignments may have been the manifestation of shallow intrusion of either a magma-filled dike or several diapirs rising from a dike.

Date and Duration of the Eruption

Date

Stratigraphic and dendrochronologic information proves that the pyroclastic phases of the North Mono eruption were completed before A.D. 1369. Radiocarbon analyses also help to constrain the date of the latest eruption of the Mono Craters to the middle of the fourteenth century.

Stratigraphic and dendrochronologic considerations described below confirm an absolute upper limiting date of A.D. 1368 for the North Mono eruption. During his study of the Inyo Domes, Miller [1985] engaged the assistance of dendrochronologist D. Yamaguchi to find the oldest trees growing upon the pyroclastic products of the latest eruption of the Inyo Domes. They found Jeffrey pines with annual growth rings as old as A.D. 1369 growing on a thick pyroclastic flow deposit that was emplaced very soon after deposition of the initial air fall blanket of the eruptive episode. A.D. 1369 is thus proven to be a minimum limiting date for the beginning of the latest Inyo eruptive episode. Miller argues that the Inyo eruption probably began only a year or two prior to A.D. 1369.

A small but appreciable sector of the initial Inyo air fall blanket fell into Mono Lake, the surface of which was at an elevation of 6406 ft (1952 m) at the time of the North Mono eruption [Stine, 1984, Figure 1]. Most exposures dug below this elevation near the southeastern shore of Mono Lake clearly display Inyo tephra atop the North Mono tephra. Typically, in these exposures the distinctive thin (<1 cm thick), dark yellowish-brown micaceous South Deadman tephra is an unreworked, normally graded ash resting conformably upon a 1- to 3-cm-thick lacustrine-reworked bed of the gray glassy unit. From this stratigraphic relationship it is quite clear that all air fall and major pyroclastic flow deposits of the North Mono eruption had been emplaced prior to deposition of the initial Inyo air fall bed. Thus the North Mono eruption had ceased prior to A.D. 1369.

At site "av," about 3 km east-northeast of Panum Dome, small twigs were collected from a bioturbated former ground surface buried by 2 m of North Mono tephra (Figure 13). These twig fragments were incorporated within this bed prior to the beginning of the eruption. The twigs provide a maximum limit of A.D. 1300 for the beginning of the eruption (Table 1).

At site "k," about 1 km south-southwest of Panum Crater, small fragments of charred wood were recovered from within the Panum Dune flow bed (Figure 13). A maximum limiting date of A.D. 1325 is provided by this date for the opening of Panum Crater.

A charred branch with bark and eight annual growth rings was collected from site "h" in the Rush Creek drainage 2 km northwest of Panum Crater. This and other small branches were found within a lapilli-rich pyroclastic flow bed above beds 1, 2, and 3 and beneath the Panum block-and-ash bed (Figure 13). It had been alive and rooted in a peaty substrate beneath bed 1 at

TABLE 1. Radiocarbon Dates Pertaining to the Most Recent Eruption of the Mono Craters

Sample no.		Type of Material	$\delta^{13}C$ °/oo	^{14}C Age[a] years B.P. ± 2σ	Calendric Date (A.D. Range)[b]	Comments
Field	Lab					
Pan-82-av-1	UW-798	< 1-cm diameter twigs	-25.26	550 ± 80	1300-1370 or 1380-1435	From site "av," within bioturbated pre-latest-eruption surficial unit, 10 cm below ground surface, blanketed by deposits of latest eruption. SW 1/4 NE 1/4 NW 1/4 sec 21 T1N R27E.
Pan-82-6	UW-799	charred small wood fragments	-24.08	530 ± 60	1325-1355 or 1390-1435	From site "k," in pyroclastic flow deposit which originated from Panum vent and directly overlies the air fall beds of the latest eruption.
Pan-82-1a	UW-797	Charred 3.5-cm diameter branch with thin bark rind and eight annual growth rings	-24.09	580 ± 60	1290 to 1420	From site "h." Rooted in organic muck at base of west bank of modern Rush Creek in SE 1/4 SE 1/4 SW 1/4 sec 13 T1N R26E. In pyroclastic flow deposit which originated from Panum vent and overlies air fall beds of latest eruption.
Weighted average of above three beds[c]				554 ± 40	1325-1365 or 1390-1420	

[a] Corrected for isotopic fractionation.
[b] Corrected for atmospheric effects according to Stuiver and Pollach [1977] and Stuiver [1982].
[c] Procedure of Long and Rippeteau [1974].

the time of the deposition of bed 1. This sample constrains the date of deposition of bed 1 and the pyroclastic flow to after A.D. 1290.

All three radiocarbon analyses yielded dates spanning most of the fourteenth and the early fifteenth centuries. At either 1- or 2-σ levels of certainty these date ranges are indistinguishable. The properly weighted average of these date ranges is A.D. 1325-1365 or 1390-1420. The dendrochronologic work described above allows us to rule out the latter period. Thus the eruption certainly was completed by A.D. 1368, and there is only one chance in 40 that the eruption occurred before A.D. 1325.

Duration

Several observations lead us to speculate that the pyroclastic phases of the North Mono eruptive episode took place during a period of no more than a few days to a few months. Furthermore, the span of time during which extrusion of the domes and coulees took place can probably be limited to a period of less than a few years.

We begin by considering evidence that places a maximum limit on the duration of the eruption. The radiocarbon and dendrochronologic data described above provide a maximum duration of about 40 years for the pyroclastic phases of the North Mono eruption. The initial eruption almost certainly occurred after A.D. 1325, and the last eruption certainly occurred before A.D. 1369.

Narrower constraints can be argued from stratigraphic evidence. All but a few of the several hundred exposures of the North Mono tephra lack any evidence for aeolian, lacustrine, or colluvial deposition or erosion between the various pyroclastic beds. For example, numerous exposures of the tephra northeast of Mono Lake, on the leeward faces of sand dunes that were active at the time of the eruption, display no aeolian beds within the planar-bedded air fall

series. This is even true at one locality where bed 1 blankets a beautifully wind-rippled dune surface. At this site ("do," Figure 4), the average rate of leeward migration of the dune can be shown to have been about 6 mm/yr for the 600 years prior to the eruption, on the basis of the horizontal separation of three late Holocene ash beds within the dune. Yet no intercalated aeolian beds occur at this and nearby sites. Similarly, sites south of the lake that display a meter or more of aeolian sand reworked from the uppermost gray glassy beds display no evidence of aeolian activity between deposition of the various planar air fall beds of the eruption. The lack of evidence for aeolian activity within the North Mono pyroclastic blanket at these sites is a strong indication that the uppermost beds of the North Mono tephra were erupted before the strong southwesterly winds common during most of the year were able to rework the underlying North Mono air fall beds. Hence we are confident that the North Mono tephra was deposited within a period of no more than several months.

Exposures of the tephra at sites where deposition occurred beneath the waters of Mono Lake also support a short eruption duration. Rates of deposition of biogenic clays at shallow water sites (now accessible because of the very low level of the lake surface) were of the order of 1 mm/yr in the 600 years prior to the North Mono eruption and have averaged 0.1-0.3 mm/yr since the eruption (S. Stine, personal communication, 1985). Of the few dozen pits exposing the tephra below the level of the fourteenth century lake, none contain evidence of erosion by lake bottom currents during the eruption or nonvolcanic lacustrine deposition within the North Mono series.

It is worth mentioning that none of the exposures studied displays evidence of sublacustrine erosion, current reworking, or biogenic deposition between pulses of the Inyo tephra eruption either. The South Deadman stratum and overlying Obsidian vent strata are quite planar bedded, and no evidence of deposition or erosion between these pulses of activity has been discovered. For this reason, we concur with Miller's [1985] assessment that the Plinian eruptions of the South Deadman (Inyo) vent and the Obsidian (Inyo) vent occurred within a period of time much shorter than the 65-year maximum limit imposed by D. Yamaguchi's dendrochronologic analysis. Indeed, the stratigraphic evidence from the shores of Mono Lake tempts us to conclude that the hiatus between these pulses of the Inyo eruption was far less than a year. This helps constrain the duration of the North Mono eruption because the Obsidian vent tephra can be found on Northern Coulee. Hence Northern Coulee, and perhaps the other flows, was extruded before A.D. 1369.

Despite the meager evidence for hiatuses during deposition of either the North Mono tephra or the Inyo tephra, clear evidence exists for a hiatus between deposition of these tephras. In all exposures that contain both of these tephra series between lacustrine beds, they are separated by a stratum of current-reworked, nonplanar-bedded, gray glassy sand with rare small pebbles of pumice. The upper centimeter of this intervenient bed has a pale olive green cast, a color common to organic-rich beds above and below the tephras. Commonly, an erosional truncation is visible at the top of the current-reworked bed, below the organic-contaminated portion.

The evidence for a hiatus between the North Mono and Inyo eruptions found in the lacustrine record is in accord with evidence found in subaerial environments. All exposures in which subaerially deposited North Mono tephra are found beneath well-bedded Inyo tephra display minor reworking of the North Mono ash. At most of these localities, well east or south of the North Mono sources, only thin laminae of the GGB were deposited. Without exception the once planar, gray glassy beds in these exposures are partially disrupted: in many cases the disruption is clearly by small burrowing animals or by rooting animals, and in some localities the beds have been partially reworked into nonplanar beds by wind action or perhaps by local running water. The overlying beds of Inyo tephra display no indications of such disturbance, except within their uppermost 20-40 cm.

From these observations it is reasonable to conclude that the time between deposition of the North Mono and the Inyo tephras was much longer than the duration of either eruption. We suspect that if the hiatus between the eruptions had been longer than a couple of years, the North Mono tephra would display more severe disruption.

Bioturbation of the lower portions of the North Mono series that can be seen at many distal sites of subaerial deposition north to east of Mono Lake places an additional constraint on the duration of the North Mono eruption. Several exposures within the sand dunes east and northeast of the lake and others in the steep, narrow canyons south and northeast of Bodie display disrupted lower beds overlain by undisturbed upper beds of the air fall series. In four canyon bottom exposures near Bodie, beds 1, 2, and 3-6 exhibit various degrees of homogenization by bioturbation (see, for example, Figure 3). The upper surface of the bioturbated zone is commonly quite planar and abruptly overlain by the undisrupted overlying planar beds, which are far-field correlatives of the GGB. The lowermost undisturbed bed is everywhere the same bed, lending greater credibility to our claim that disruption occurred just prior to its deposition. The bioturbation at these sites occurred after deposition of beds 3-6 but before deposition of the GGB. In the dunes northeast and east of Mono Lake, beds 1, 2, and 3-6 commonly have been homogenized beyond recognition and are overlain by undisturbed bed 7 and the GGB. Taken together, these dozen or so sites indicate a period of shallow disruption by biological agents between deposition of beds 6 and 7. This period would correspond to a time before, during, or just after deposition of the very thin air fall and pyroclastic flow beds between beds 6 and 7 near the source vents (see Figure 2).

Several other observations should be mentioned before assessing the nature of this disruption and the time it represents. (1) Not the slightest hint of biogenic, aeolian, or fluvial activity has been found at this horizon within 20 km of the source vents, where the initial air

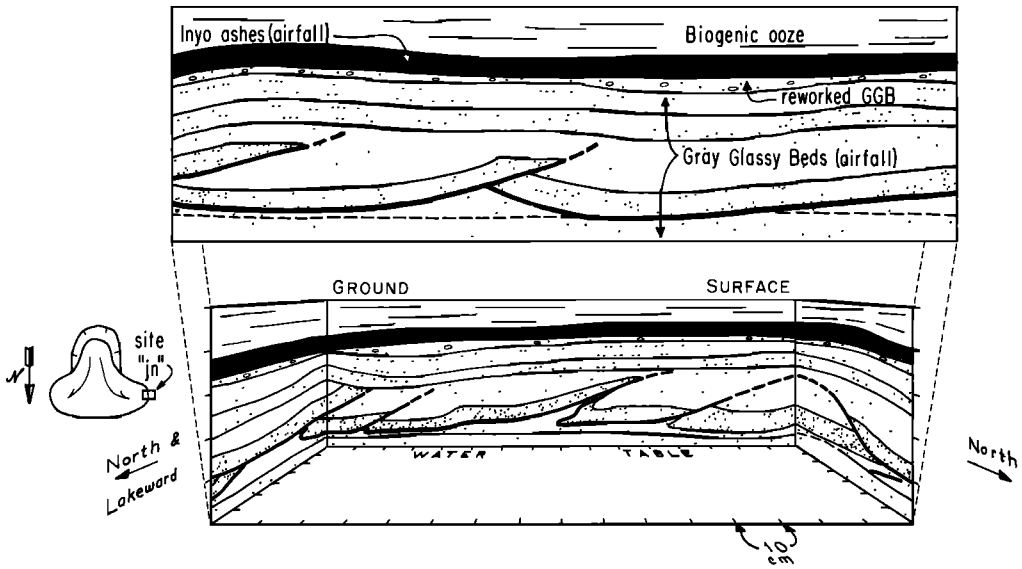

Fig. 17. This perspective sketch of excavation "jn," on the southern margin of Mono Lake, shows imbricate bedding-plane faults and ramp thrusts within the gray glassy beds of the North Mono tephra. The uppermost 10 cm of the GGB were deposited subsequent to this deformational episode (event 1), which most probably occurred in response to a strong seismic shock. Ground surface here is at about 6384 feet (1946 m), about 22 feet (6.7 m) below the surface of Mono Lake at the time the deformation occurred. The lowest 40 cm of North Mono tephra are below water table at this site. Inset shows, in plan view, plausible location of this exposure on the flank of a lateral spread beneath the waters of Mono Lake.

fall beds are more than about 5 cm thick. (2) The white pumiceous grains of the disrupted thin air fall beds have not been mixed deeper than a few centimeters into the substrate. (3) Evidence of aeolian or fluvial activity does not accompany the evidence of homogenization. (4) The uppermost distal air fall beds commonly are in abrupt, planar contact with overlying aeolian sand (northeast and east of the lake) or a massive ash-rich debris flow bed (in the canyons near Bodie).

These four observations lead us to conclude that the homogenization of beds 1, 2, and 3-6 was produced by animals in search of food after deposition of the initial Plinian air fall blanket (beds 1-6). From observation 1, either these animals were killed or died of starvation within the thicker, near-field tephra blanket, or their initial attempts to uncover food beneath the air fall blanket were unsuccessful and they left for greener pastures. From observation 2 these animals did not disrupt the thin ash blanket principally by burrowing but rather by rooting in the thin ash in search of edibles. From observation 3 the hiatus was too short to allow reworking of the thin ash by aeolian or other nonbiological agents. As discussed above, this probably limits the hiatus to less than a few weeks or months. Observation 4 indicates that the animals either did not remain or did not survive within the area of the distal air fall blanket after deposition of bed 7 and the GGB.

Seismicity Associated With the North Mono and Inyo Eruptions

In the course of study of the North Mono and Inyo tephras, clear evidence of soft-sediment deformation was exposed in several pits around the perimeter of Mono Lake. This deformation, which most probably records seismic shaking associated with volcanic activity in the Mono and Inyo craters, presents an intriguing opportunity for further study of the relationship between tectonism and volcanism in the region.

Between about A.D. 700 and 1369 at least seven distinct episodes of soft-sediment deformation related to liquefaction took place in the sediments of Mono Lake. The two oldest of these took place well before the North Mono eruption and have been discussed briefly by Wood and Stine [1984]. The remaining five events, which took place during the eruption of the North Mono and Inyo tephras, are the subject of the following discussion.

The liquefaction phenomena associated with the latest eruptions of the Mono and Inyo Craters are of three types: (1) bedding-plane faults and associated ramp thrusts, (2) load casts and diapiric structures, and (3) sandblows. These features were found at the four sites labeled "gf," "jl," and "jn" in Figure 5 and "dk" in Figure 4. At the time of their formation the level of Mono Lake was about 6406 ft (1952 m), more than 20 ft (6 m) above each of these sites [Stine, 1984, Figure 1].

The first of the five recognized episodes of liquefaction (event 1) occurred late in the eruption of the North Mono tephra. Figure 17 illustrates one of the four pits in which features associated with event 1 were uncovered. In this perspective diagram, all four vertical walls of the pit display spectacular evidence of slip along bedding-plane and ramp thrust faults within the GGB. Strike of the faults is variable but approximately

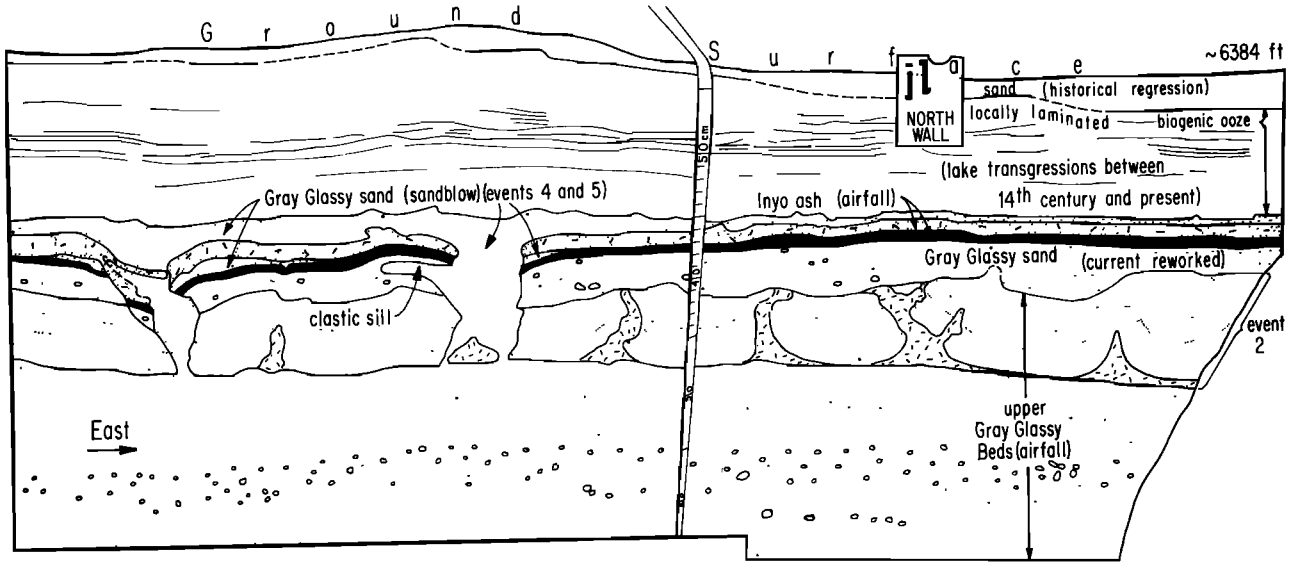

Fig. 18. Portion of north wall of exposure "j1," on south shore of Mono Lake, shows liquefaction events 2, 4, and 5, which occurred after deposition of the North Mono tephra and in conjunction with deposition of the Inyo tephra. Black band is Inyo ash from South Deadman vent. Overlying dense dot pattern with short dashes is Inyo ash from vent under Obsidian Dome.

north-south. All faults initiated movement at the base of the same stratum within the lower portion of the GGB. Failure apparently began along one contiguous bedding plane; that fault plane was later imbricated and locally overturned as each fault segment overrode its western neighbor. This imbrication resulted in an east-west shortening of the exposed part of the overlying sedimentary blanket by 1.2 m. Note that the direction of shortening is parallel to contour, not downslope.

This "thin-skinned" failure continues beyond the limits of the exposure, but its total dimension is unknown. The position of the exposure within the overall failure is also conjectural. However, the structures probably represent a portion of a lateral spread, that is, a thin blanket of sediment that moved horizontally on a liquefied substrate (for other examples, see Keefer [1984, p. 418]). Quite possibly the exposure is located on the western margin of the toe of a lateral spread, as suggested in the inset to Figure 17. Considering that three of the pits dug on the southern, northern and eastern shores of the lake ("dk," "gf," and "jn") revealed evidence of lateral spreading, these and contemporaneous failures must have covered a large percentage of the lake floor.

An estimate of the size of earthquake necessary to produce these lateral spreads is possible using the empirical relationships developed by Youd and Perkins [1978] and by Keefer [1984]. They demonstrated from historical observations that the distance from earthquake source to most distant lateral spread is related to earthquake magnitude (M_S). They conclude that quakes with magnitudes less than 5.0 do not produce liquefaction. The major problem in this case is identifying the source of the earthquake. Perhaps the most logical guess is that the causative quake was produced by slippage beneath the source vents for the North Mono tephra because the event occurred during the North Mono eruption. The most distant evidence for lateral spreading is on the north side of the lake, about 17 km from the source vents. Lateral spreads are produced at such distances only during earthquakes of $M_S \geq 6.5$ [Keefer, 1984, Figure 3c]. The minimum distance from source to lateral spread is half the distance between the two most widely spaced sites. This distance, 7.5 km, corresponds to an earthquake of magnitude 5.5 or greater.

Evidence for the second deformational event (event 2) is not present in the pit illustrated in Figure 17 but is apparent in another pit on the southern shore of the lake. Figure 18 illustrates a portion of the northern wall of that excavation, and Figure 19 displays a portion of the western wall. Event 2 is indicated by load casts of laminated sand and intervenient diapirs of silty sand in the upper few centimeters of unreworked gray glassy beds. Prior to deformation the silty sand resided as an air fall bed of uniform thickness beneath the laminated sands. This silty bed apparently was less dense than the overlying sand and rose diapirically through the sand. This occurred prior to final reworking of the uppermost sands by lacustrine bottom currents, judging from the fact that reworked sand overlies the deformed bed and truncates diapirs and laminae. In many instances, such structures are known to have formed in response to strong seismic shaking. Sims's [1973] studies of such features suggest that Modified Mercalli intensities $\geq$ VIII are necessary to produce penetrative deformation of this sort. Such high intensities are not common for earthquakes of $M < 6$. Thus the magnitude of

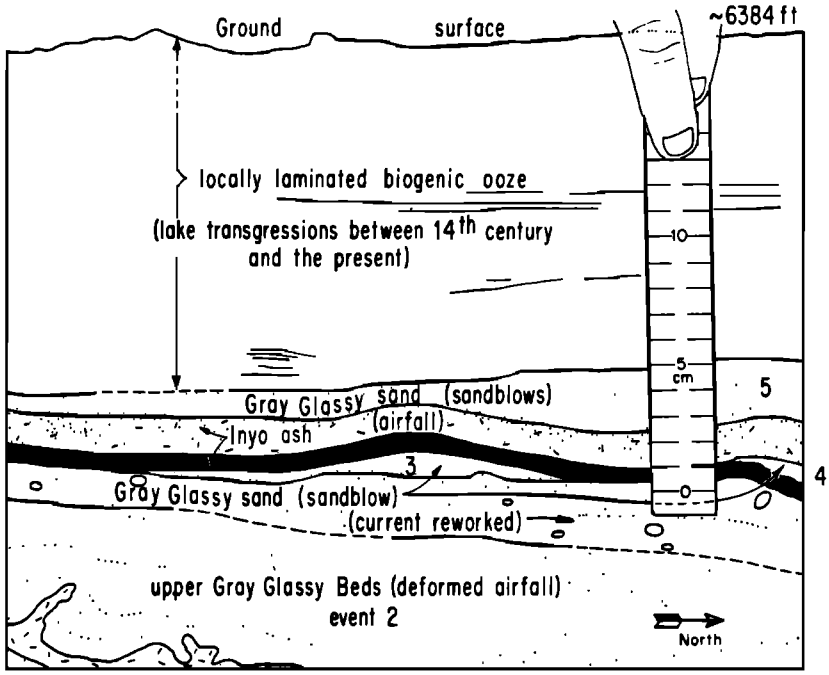

Fig. 19. Portion of west wall of exposure "j1" shows liquefaction episodes 2, 3, 4, and 5 which occurred after the deposition of the North Mono tephra and before, during, and after deposition of the Inyo tephra.

event 2, which occurred soon after the deposition of the GGB, probably was M > 6.

Liquefaction events 3, 4, and 5 left a record of clastic dikes and sandblows. Event 3 is represented in these illustrations by only one small sandblow located between the reworked layer of Mono Craters sand and the lower Inyo tephra, which was erupted from the South Deadman vent and is shown in solid black in Figure 19. In cross section the sandblow feature is a 1-cm-thick, 18-cm-wide wedge of Mono Craters sand. In plan view the body is nearly circular. Several other isolated small bodies of similar size and shape were uncovered at this same horizon by incrementally cutting several tens of centimeters into the wall illustrated in Figure 19. Their circular shape and central peak preclude an origin related to flow of lacustrine currents over the lake bottom. Their razor-sharp margins argue against an intrusive origin and in favor of production by expulsion onto the lake bottom from an underlying unit. Furthermore, this is a common seismically induced phenomenon in water-saturated sands and coarse silts.

Significantly, the sandblows were deposited directly upon a unit that displays clear evidence of reworking by lake bottom currents, and yet the sandblows show no evidence whatever of modification by currents after construction upon the lake bottom. In addition, the sandblows are not capped by even the thinnest coating of biogenic ooze. Apparently, the South Deadman (Inyo) ash blanketed the sandblows very soon after they formed.

From this evidence a reasonable conjecture is that a moderate to large earthquake closely preceded deposition of the South Deadman (Inyo) ash. This possibility is particularly intriguing in light of the fact that the Inyo Craters lie along the surficial trace of the Hartley Springs fault, the principal structure that demarcates the eastern Sierran front. Could it be that an earthquake produced by slippage on that fault heralded the beginning of the South Deadman (Inyo) eruption? If so, and if Youd and Jenkins's [1978] and Keefer's [1984] distance versus magnitude curves for liquefaction failures are applicable to small sublacustrine sandblows, the size of the event would have been $M_s > 6.5$.

Similar sandblows also were deposited on top of the South Deadman (Inyo) ash. Part of one such blow is visible at the right margin of Figure 19. The flanks of two other small sandblows resting upon the South Deadman (Inyo) ash are also visible on the left side of Figure 18. The centers of these two structures, however, were removed during later expulsion of sand from the same two vents. Once again the sharp, feather edges argue against intrusion and for construction upon the lake bottom. By contrast, one blunt finger of sand projecting toward the left, below the South Deadman (Inyo) ash, in Figure 18 is clearly an intrusion, a clastic sill. The sandblows overlying the South Deadman (Inyo) ash are clearly sandblows because they are composed exclusively of gray glassy Mono Craters ash, even though they rest upon a contiguous blanket of micaceous, dark yellowish-brown Inyo ash. If these cones of sand had formed by current-reworked lake bottom sand, they would be composed of Inyo, not Mono, sand.

These small sandblows fell directly upon an unreworked blanket of South Deadman (Inyo) ash and were covered undisturbed by Obsidian vent (Inyo) ash. The lack of reworking above or below the sandblows implies that the sandblows and the Obsidian vent ash were deposited very soon, perhaps no more than a few hours or days, after

eruption of the South Deadman (Inyo) ash. A reasonable hypothesis would be that further slippage on the Hartley Springs fault produced a second moderate earthquake that heralded the opening of Obsidian vent and the Plinian eruption of its tephra. This speculation could be tested by studying exposures of the Inyo tephra across the Hartley Springs fault.

The fifth and youngest of the recognized liquefaction events occurred after deposition of the Obsidian vent (Inyo) ash. This event resulted in deposition upon the lake bottom of a much larger volume of North Mono sand than did the two preceding events, 3 and 4, and it left the two prominent feeder conduits shown in Figure 18. Sand expelled onto the lake bottom during event 5 clearly was derived from the crudely laminated gray glassy sand about 10 cm beneath the lake bottom.

In conclusion, five earthquakes of at least moderate size shook the southern shore of Mono Lake during the North Mono-Inyo eruptions. One of these occurred during the final stage of the North Mono eruption. Another occurred after that eruption ceased and before deposition of reworked tephra. A third earthquake occurred after the North Mono ash had been slightly worked by lacustrine currents but immediately prior to deposition of the South Deadman (Inyo) ash. A fourth earthquake followed soon after deposition of this ash and closely preceded deposition of the Obsidian vent ash. A fifth earthquake occurred after deposition of the Obsidian vent ash.

The indications of strong earthquakes closely related to the North Mono-Inyo eruptions suggest that studies of the tephra-mantled faults in the vicinity of the Mono and Inyo craters could be quite productive. Perhaps one could determine that the Hartley Springs fault ruptured just prior to the opening of the South Deadman and Obsidian vents or that faults west and east of the Mono Craters moved in response to the evacuation of magma during the North Mono eruption.

Discussion

Several aspects of the North Mono eruption warrant additional attention because of their value for understanding volcanotectonic processes and the potential for future eruptions in the region. In this section we conclude that (1) the North Mono dike intrusion relieved accumulated tectonic extensional strains by elastic rebound, (2) magma pressure must have been high enough to force the dike walls even farther apart than would be expected from elastic rebound alone, (3) the pulsating nature of the Plinian eruption resulted from incremental release of the water-rich rising magma dike, and (4) the gradually diminishing explosiveness of the eruption was probably a consequence of vertical stratification of water within the magma dike.

Plausible Causes of the North Mono Dike Intrusion

Although the geometry, evolution, and timing of the North Mono eruption are now well known, the cause of the eruption is not. In this section we attempt to constrain the numerous possibilities.

The North Mono eruption is the latest in a 35,000-year-long series of moderate eruptions of high-silica rhyolites. This latest eruption contributed 0.44 km^3 (or about 5%) of the total (8.7 km^3) volume of the Mono Craters. The compositional similarity, size, and continuing construction of this volcanic edifice suggest the presence of an active magma reservoir in the subjacent crust. Achauer et al. [1984] claim to have located this reservoir about 10–20 km beneath the Mono Craters using teleseismic P wave residuals.

The North Mono eruption and its many predecessors must have occurred at times when small amounts of magma were able to ascend from this reservoir through the upper crust to the earth's surface. To have successfully accomplished this ascent, magma in the reservoir must have achieved pressures adequate for initiating and propagating a fracture through the overlying rocks. In addition, the magma in the fracture must have ascended to the surface rapidly enough to avoid freezing within the fracture.

In this region of active tectonic extension, one must consider the possibility that dike intrusions are aided by the inexorable elastic stretching that occurs in periods between brittle, seismic failure of the crust. In fact, dike intrusion in such a setting might well be a means for relieving elastic strain accumulation, in a manner akin to the seismological phenomenon of elastic rebound. Other plausible mechanisms for initiating an eruption would involve sudden or steady buildup of magma pressures within the reservoir by magma mixing.

Three observations guide the discussion of these mechanisms below. First, the sparsity of nonjuvenile material among the products of the North Mono eruption indicates that rising magma did not remove large amounts of country rock to make room for its ascent through the crust. Second, the North Mono and Inyo dikes and the Mono Craters edifice itself strike roughly perpendicular to the direction of regional least principal stress. Third, the paucity of Holocene and late Pleistocene fault scarps along the Sierran front west of the Mono Craters suggests that shear faulting no longer serves so important a role in relieving elastic strain as it had in former times.

Lack of erosion of wall rock. An argument against ascent of the North Mono dike by assimilation or erosion of overlying crustal rocks arises from the observation that the material evacuated through the North Mono source vents contains only a very small percentage of angular plutonic clasts. We estimate that such clasts, which could represent crustal host rock torn from conduit walls well beneath the source vents, constitute about 0.1% or less of the total volume of the erupted products. This would be equal to a volume of no more than 660,000 m^3, which, if eroded from the walls of a dike 4 km long and 10 km deep, would represent a thickness of $\leq$17 mm. The vent erosion that can be demonstrated (to produce, for example, bed 7 and the Panum throat-clearing breccia) was shown above to have occurred in the shallow subsurface.

The lack of evidence for erosion of granitic country rock during intrusion and extrusion of

the North Mono dike can be interpreted in one of two ways: either (1) eroded granitic fragments could have settled downward through the rising rhyolitic magma and hence would not have been incorporated into the extruded tephra and lava or (2) country rock was moved laterally out of the way of the intruding dike, obviating the need for fragmentation and transport by the magma. Settling velocities calculated from Stoke's law for pebble- to small boulder-sized granitic fragments ($\rho \approx 2.65$ g/cm^3) through rhyolitic melt ($\rho = 2.4$ g/cm^3) with a dynamic viscosity μ of 10^6-10^9 P are of the order of 10^{-4} to 0.1 cm/s, more than 3 orders of magnitude slower than rates of magma ascent calculated below. This suggests that settling of clasts through the rising North Mono magma is improbable; country rock must have moved aside as the magma dike rose.

Regional strain pattern. The Mono Craters lie at the edge of the Basin Ranges, a geologic province characterized by young, narrow, north-south trending mountain ranges and intervening valleys. These fault-bounded and tilted landforms are clear evidence of continuing east-west crustal extension throughout the past several million years [Gilbert, 1928]. During the periods of both historical and prehistoric record, elastic straining across the Basin Ranges has been relieved locally by large seismic episodes of normal faulting (see, for example, Wallace [1981]) according to the theory of elastic strain accumulation and rebound first proposed by Gilbert [1884] and later elucidated by Reid [1910].

Although no measurements of contemporary elastic deformation across the Mono Basin have been undertaken, geodetic measurements of the Excelsior network, east of the basin, indicate appreciable east-west extension during the period 1972-1978 [Savage, 1983]. Furthermore, geodetic measurements to the south clearly indicate that regional northeast-southwest extension has been taking place across the Long Valley caldera during the recent period of geologic unrest that began in 1978 [Hill et al., 1985].

Moreover, geologic data confirm a long-lived environment of east-west extension in the region of the Mono Craters. Normal faults of Quaternary age to the south, northwest, and east trend north-south to northwest-southeast (Figure 1); these orientations indicate an east-west to northeast-southwest orientation of the regional least principal stress.

The orientations of fissures and faults associated with the North Mono and Inyo eruptions are quite compatible with these regional patterns of elastic and permanent strain. As is common in other regions of dike intrusion, these features strike approximately perpendicular to the regional least principal stress. This geometrical relationship renders north-south dike intrusion a plausible companion or alternative to normal faulting as a mechanism for elastic rebound and permanent crustal extension in this region.

Sparsity of young Sierran frontal faults. A third observation also is important in understanding the mechanism of emplacement of the North Mono dike. In the Mono Basin and adjacent regions, hundreds of meters of east-west extension have occurred along the normal faults of the eastern Sierran front within the past several million years [Curry, 1971]. Curiously, however, evidence of extensional faulting during the past few tens of thousands of years is subdued to absent along the Sierran front west of the Mono Craters (Figure 1). In spite of the cessation of normal faulting along the range front, we have no reason to believe that extension of the Mono Basin has slowed or ceased. Therefore a reasonable hypothesis is that dike intrusion beneath the Mono Craters has become the dominant means by which shallow crustal extension occurs in this region.

Calculations. If magma is to rise by buoyancy alone through a conduit and eventually erupt, it must rise rapidly enough to avoid freezing en route due to heat loss to the wall rock. With the guidance of D. Stevenson, we have made some simple calculations in order to see what dike widths and magma rheologies are plausible in the case of the North Mono eruption.

Magma will rise buoyantly through a crack at a velocity that is proportional both to the density contrast between the magma and the host rock and to the square of the dike width. More significantly, the velocity of ascent is inversely proportional to the viscosity of the magma, which, in turn, is a function of both magma temperature and water content. Turcotte and Schubert [1982] derived the following equation for the buoyant rise of viscous magma in a dike of infinite length:

$$V = \frac{g\Delta\rho}{\mu}\left(\frac{d^2}{8} - \frac{y^2}{2}\right) \qquad (1)$$

where

- V velocity of ascent;
- g 980 cm/s^2;
- $\Delta\rho$ $\rho_{\text{host rock}} - \rho_{\text{magma}}$;
- d dike width;
- μ magma viscosity;
- y distance outward from central plane of the dike.

Equation (1) assumes laminar flow of magma in the dike; hence the velocity profile is parabolic: magma at the center of the dike ($y = 0$) will move more rapidly than magma adjacent to the walls. The density contrast $\Delta\rho$ in this case is about 0.25 g/cm^3. (We can assume that the density of the granitic host rock is about 2.65 g/cm^3, and we have direct measurements of 2.4 g/cm^3 for glassy pyroclasts of the eruption.) The only data on temperature of the magma in the reservoir are Fe-Ti oxide temperature determinations of 900°C for a sample of Cratered Dome and 815°C for a sample of Northern Coulee [Carmichael, 1967]. The water content of obsidian clasts in the erupted magma ranges from 2.6 wt % to about 0.2 wt % [Newman et al., 1986]. For rhyolitic magma with these temperatures and water contents, Murase [1962] and Carmichael et al. [1974] derive viscosities μ ranging between 2×10^6 and 2×10^9 P.

Credible dike widths for a purely elastic rebound mechanism can be estimated by considering the geologic setting and strength of the crustal rocks involved. In the Basin Ranges province, historical episodes of normal faulting have resulted in horizontal coseismic rebound of 1-3 m

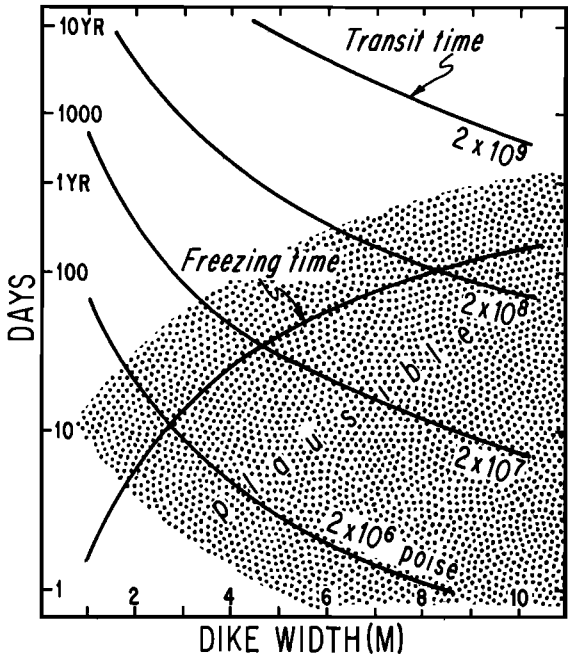

Fig. 20. Range of plausible dike widths and viscosities for the North Mono eruption calculated from equations for heat loss and buoyant rise of magma in a dike.

(for example, see Whitten [1957] and Stein and Barrientos [1985]). One would expect, therefore, that a dike could relieve elastic strains no greater than these values because normal faulting would occur if strains exceeded these values. Maximum ascent velocity for water-poor magma (μ = 2 x 10^9 P) is 1.5 x 10^{-4} cm/s in a 1-m-wide dike. Ascent velocity for water-rich magma (μ = 2 x 10^6 P) is 1.5 x 10^{-2} cm/s.

Transit times to the surface for the various magmas can now be calculated if the depth to the top of the magma reservoir can be estimated. Achauer et al. [1984] argue from their tomographic inversion of teleseismic P wave residuals that a magma body exists beneath the central one third of the Mono Craters at depths between 10 and 20 km. Therefore let us assume that the depth to the top of the magma reservoir is 10 km. Figure 20 shows transit times calculated using this value that range from less than one day (for the most fluid magma in a 10-m-wide dike) to much more than 10 years (for the most viscous magma in a 1-m-wide dike).

As magma rises in the dike, heat will be lost to the cooler host rock. If the magma is to reach the earth's surface, its transit time must be shorter than the time required to freeze it by transfer of heat into the host rock. According to Murase [1962], decreases of temperature by about 100°K will result in increases in viscosity of about an order of magnitude. From equation (1), then, one can estimate a concomitant drop in ascent velocity of about an order of magnitude for every drop in temperature of 100°K. As a crude measure of whether or not a dike will be able to reach the surface and erupt, we will assume that it must rise fast enough to avoid a decrease in temperature of 100°K.

The diffusion of heat from a stationary magma dike would occur according to the diffusion equation [Turcotte and Schubert, 1982, p. 160]:

$$T = T_{magma} + (T_{wall} - T_{magma})\ \mathrm{erfc}\left(\frac{\frac{d}{2} - y}{2\sqrt{\kappa t_f}}\right) \quad (2)$$

where

- T temperature (in degrees Kelvin) at a point $(d/2) - y$ into the dike from the wall;
- κ thermal diffusivity $\approx 10^{-2}$ cm^2 s^{-1};
- t_f time to lower the magma temperature by 100°K;
- T_{wall} temperature of the dike wall $= (T_{magma} - T_{country\ rock})/2$

To simplify further, we calculate the magma cooling rates halfway between the ground surface and the top of the magma reservoir, that is, at a depth of 5 km. Rates of cooling above this depth will be faster, and rates below this depth will be slower. Extrapolation of the surficial thermal gradient of 31°K/km [Lachenbruch et al., 1976] yields a temperature of roughly 500°K at 5 km.

Our calculations are summarized in Figure 20, which shows the freezing time t_f for dikes ranging in width from 1 to 10 m. The calculated times range from 1.5 days (for the narrowest dike) to nearly a year (for the widest dike).

By comparing the freezing times with the transit times in Figure 20, one can crudely assess the range of plausible widths and viscosities for the North Mono dike. Magmas in dikes 2 m or less in width appear to be implausible because their transit times are very much longer than their freezing times. For the most tectonically plausible dike widths (<3 m), only high-water magma ($\gtrsim$2.6 wt % H_2O; $\mu \lesssim 2 \times 10^6$ P) appears capable of rising with enough rapidity to avoid freezing within the conduit. Eruption of slightly more viscous magma is plausible if one allows for the fact that the initial magma will transfer heat into the country rock and thereby reduce heat losses for the magma ascending after it. Even under these conditions, only magmas with viscosity $\lesssim 10^7$ P (~2.0 wt % H_2O) would be able to reach the ground surface prior to freezing and erupt from the widest credible dike produced solely by elastic rebound of tectonically accumulated strains.

Thus it appears that dike widths produced by tectonic processes alone would have been too narrow to enable the eruption of all but the initial Plinian deposit (bed 1) of the North Mono eruption. Within the range of dike widths shown in Figure 20, the most plausible width for the North Mono dike is about 10 m. And yet, no more than about 3 m of this could have been acquired by elastic rebound. For this reason, one must consider means of producing either a wider dike or more rapid ascent.

Sparks et al. [1977] suggest that some rhyolitic magmas have been induced to erupt by injection of hotter mafic magma into a rhyolitic magma reservoir. An overpressured magma resulting from this process might then be able to produce tensile failure in the overlying rock and

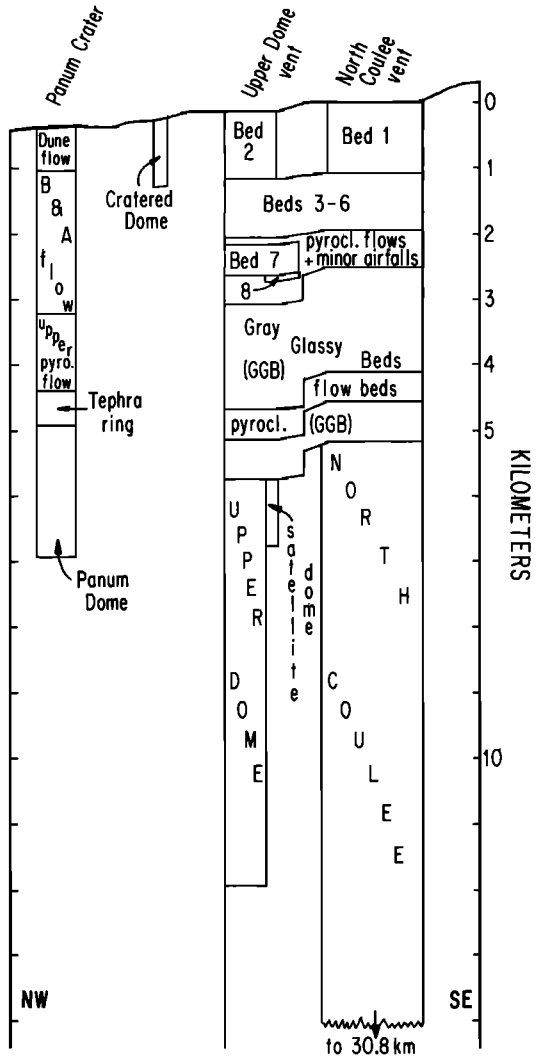

Fig. 21. Cross section in the plane of the North Mono dike showing hypothetical arrangement of the many erupted units. No vertical exaggeration. Dike width of 10 m is assumed.

propagate a dike to the surface. The upward velocity of magma in this case would be greater than that produced solely by buoyant rise, and the width of the dike produced would be greater than that allowable by elastic rebound alone. Thus narrower and more viscous dikes could reach the surface.

Speculations Concerning the Nature of the Eruption

We turn now from discussion of the North Mono dike intrusion to a consideration of the eruption of that dike. In particular, we wish to examine the two dominant characteristics of the eruption: its discontinuous, pulsating nature, and its progression from a Plinian phase to a pyroclastic flow phase to a dome-building phase. In these two aspects the North Mono eruption is like many other silicic volcanic eruptions; hence conclusions from the study of this eruption may well be more generally applicable.

Arrangement of units in the dike. We begin by considering the configuration of the many erupted units in their dikes prior to the initial opening of each vent. Figure 21 is a hypothetical cross section drawn in the plane of the dikes which shows a plausible arrangement of the units, arranged beneath the vent or vents from which they were expelled, in the order of their expulsion. For example, bed 1, which was the first unit out of its vent, is placed at the top of its dike, and Northern Coulee, the last unit out of the vent, is placed at the base. In constructing the cross section we have assumed that each dike extends downward from the various vents with vertical northwestern and southeastern edges. We have also assumed a uniform dike width of 10 m for each dike. This width is somewhat greater than the 7.3 m width of the Inyo dike recently intersected 700 m beneath the ground surface between the Inyo Domes by slant drilling [Eichelberger et al., 1985] and is also at least 3 times greater than the maximum width consistent with an elastic rebound mechanism. This width does, however, yield rates of ascent for both early and late erupted products that are most consistent with estimated eruption durations for this and historical silicic eruptions. To calculate the vertical thickness of each unit within its dike, we have divided its volume by the dike's length in the plane of Figure 21 and by its assumed width of 10 m. Table 2 lists the various units, sources, and volumes used to construct Figure 21. Dense-rock-equivalent volumes have been calculated for the pyroclastic fall and flow beds using an experimentally determined reduction factor of 0.4.

The most striking feature of the hypothetical cross section is that the main dike would extend to a depth of over 30 km, about 3 times deeper than the top of the magma reservoir proposed by Achauer et al. [1984]. Hence we conclude that much of the erupted North Mono magma was still within its magma reservoir during the Plinian phases of the North Mono eruption. In fact, magma probably was still exiting the reservoir at the base of the dike when the first extrusions of Northern Coulee began.

Water content of obsidians. In the context of the preceding discussion we now consider the volatile content of the products of the North Mono eruption. The North Mono eruption evolved in a manner that is common to many silicic eruptions. That is, it progressed from an initial episode of violent Plinian eruptions through a time of less explosive ash flow eruptions to a period of relatively passive extrusion of thick domes and lava flows. The durations of the most explosive phases of the eruption are probably measured in hours. The extrusion of the domes probably took place episodically over a period of several months to several years, judging from observations of similar extrusions elsewhere in the world.

Stratification of volatiles within the volcanic conduit has commonly been called upon to explain the gradual diminishing of explosiveness during eruption of silicic magmas [Williams and McBirney, 1979]. The decreasing violence of successive phases of the eruption might be an expected consequence of lower volatile content of the deeper magma. A downdip decrease in water

TABLE 2. Volumes and Sources of Deposits of the North Mono Eruption

Unit	Sources	Volume[a]	(DRE)[b], km^3
Air fall beds			
Bed 1	9-10	0.038	(0.015)
Bed 2	3-5	0.018	(0.007)
Beds 3-6	3-10	0.065	(0.026)
Bed 7	3-7	0.012	(0.005)
GGB	3-10	0.164	(0.066)
Others	3-10	0.123	(0.049)
Total		0.420	(0.168)
Pyroclastic flow deposits			
West flow deposit	9-10	0.050	(0.020)
Undifferentiated flow deposit	3-10	0.019	(0.008)
Panum Dune flow deposit	1	0.009	(0.004)
Panum block-and-ash flow deposit	1	0.033	(0.013)
Panum uppermost flow deposit	1	0.017	(0.007)
Total		0.128	(0.052)
Domes and coulees			
North Coulee	9-10	0.385	
Upper Dome	3	0.037	
Satellite dome and tephra ring	3-4	0.002	
Cratered Dome	2	0.002	
Panum Dome	1	0.012	
Panum tephra ring	1	0.003	(0.001)
Total			(0.439)

[a] Includes only that portion within 130 km of the source vents.
[b] Dense-rock equivalent volume has been calculated by multiplying actual volume by 0.4. Analysis of several near-field and far-field beds gave densities in the range 0.8-1.0 g/cm^3, and analyses of North Mono obsidians gave densities of 2.3-2.4 g/cm^3. The volume of each pyroclastic blanket determined from the isopach maps should therefore be reduced by a factor of 0.3-0.4 to obtain its volume in the dike prior to vesiculation and fragmentation.

content in a buoyant dike would result in a downdip increase in magma viscosity and hence a progressive decrease in the rate of buoyant rise of later batches of magma.

Variations of water content among the units of the North Mono eruption ostensibly support this general model. The water content of obsidian pyroclasts of the North Mono eruption decreases systematically from early to late erupted products [A. Fuad and G. Rossman, unpublished data, 1982; Newman et al., 1986]. The values, measured by manometry, range from 0.1 to 2.6. Obsidian from bed 1, the initial deposit of the eruption, has about 2.6 wt % water. Water content of bed 2 obsidians averages 1.6 wt %. In gray obsidians from the gray glassy beds, water content is about 0.7 wt %. And water content for obsidians of the various domes and coulees ranges from 0.1 to 0.3 wt %.

One complication arises in attempting to interpret these data as evidence for original stratification of water content within the rising magma dike: the physical location of the analyzed obsidian pyroclasts in the dike prior to eruption is uncertain. Hence it is uncertain that the obsidian water contents are representative of the original water contents of the magma.

Our only clues to preeruptive position of the analyzed obsidians are the analogous obsidians in unfragmented domes and coulees and the percentage of obsidian in the various beds. Perhaps the most reasonable judgment is that the samples constituted a thin rind of obsidian that developed along the walls and roof of the rising magma dike. Detailed mapping of Northern Coulee, Southern Coulee, and other flows [Kelleher, 1986] shows that a thin but massive obsidian carapace surrounded the pumiceous to stony interiors of these magma bodies prior to their extrusion. The south dome of Panum Dome, described above, also has a carapace of massive obsidian. This 1-m-thick layer lies between the pumiceous to stony interior of the south dome and the older dome rocks pushed out of the way by the rising south dome. The volume of the obsidian carapace on the south dome of Panum Dome is roughly 2% of the total volume of the south dome, about the same percentage of massive obsidian as is seen in the pyroclastic fall beds.

Obsidian carapaces might have formed by quenching of that part of the magma that was

juxtaposed against relatively cool country rock. If this quenching occurred below the level at which water is saturated in the magma, the obsidian could be expected to retain the water contained by the magma during ascent from its reservoir; if quenching occurred above the water saturation depth of the magma, the obsidian would have formed on the margins of a vesiculated froth of melt and bubbles. If this obsidian was derived from vesiculated froth from which the water-vapor-rich bubbles were able to escape, as suggested by Taylor et al. [1983], then the water content of the obsidian would be less than the original content of the magma prior to vesiculation. The mechanism for removing this water from the obsidian would be problematic, however, because the viscosity of the melt would probably be far too high to allow migration of bubbles out of the melt by buoyancy [Sparks, 1978].

Vesiculation of the magma above its water saturation depth and the development of excess pressure. Consider now the response of the magma of the first erupted unit, bed 1, as it rose upward in its dike. When this batch of melt began its buoyant rise through the crust, its temperature may well have been about 900°C [Carmichael, 1967], and its water content probably was at least 2.6 wt %. These would have given it a viscosity $\mu \leq 2 \times 10^6$ P [Murase, 1962; Carmichael et al., 1974]. Given this viscosity, its ascent velocity through a 10-m-wide dike would have averaged > 15 cm/s, and its transit time through the crust would have been < 18 hours.

If one assumes that the magma contained 2.6 wt % H_2O, bed 1 magma would have been undersaturated until it had risen to a level at which the lithostatic pressure was about 400 bars [Shaw, 1974; L.A. Silver, unpublished data, 1986]). This would be the overburden pressure at a depth of about 1500 m beneath the ground surface.

When the magma of bed 1 rose a few meters above that level, vesiculation would have commenced [Sparks, 1978]. As the magma rose still higher, the vapor pressure of dissolved water in the melt would have continued to equilibrate with the decreasing lithostatic pressure by diffusion of water into the growing bubbles. During this time the pressure in the bubbles would have been maintained at values close to lithostatic pressure by bubble growth as the magma froth rose. If equilibrium between vapor pressure in the degassing melt, gas pressure in the bubbles, and overburden pressure could have been maintained by continued diffusion into the bubbles and bubble growth as the magma froth approached the surface, no Plinian eruption would have occurred. Gas pressures in melts of viscosity $\geq 10^6$ P are not believed to maintain such equilibrium, however, because diffusion of water out of such melts significantly increases their viscosity, with the result that bubbles commonly cease growing well before eruption [Sparks, 1978].

The lineated nature of bubbles within the pumiceous tephra of bed 1 clearly demonstrates, in fact, that bubbles did cease growth well before the magma froth ceased rising within its conduit. The measured densities of air fall pumice pyroclasts (ρ = 0.7–1.6 g/cm^3) indicates that the magma froth ceased expansion upon reaching a volume of 50–300% greater than its volume prior to vesiculation.

Once the gas pressures were unable to be relieved by continued expansion of the bubbles, the pressure within the bubbles in the still rising magma froth began to exceed the diminishing overburden pressure. It was these excess pressures which eventually exceeded the tensile strength and surface tension of the magma froth and resulted in its violent fragmentation and the Plinian eruption of bed 1.

The eruption of bed 1 occurred through one or more narrow fissures, in the area of source 9 (Figure 15). That the fissures were narrow can be deduced from the fact that the magma froth which fragmented to produce bed 1 does not appear to have excavated a large crater either before or in the course of its eruption. Exposures within half a kilometer of the source(s) reveal no accidental- or accessory-rich breccia beds beneath bed 1.

Accessory volcanic fragments interspersed with juvenile pumice are common, however, in the lower half of bed 1 at near-field sites. These fragments are dark gray aphyric to sparsely porphyritic dull glassy clasts that may well have been derived from dome 14 [Wood, 1977a, 1984], the mid-Holocene dome underlying Northern Coulee which must have been penetrated by the rising magma of bed 1. The volume of this material in bed 1, about 2×10^{-4} km^3, may indicate a widening of the bed 1 conduit to form a slightly wider fissure, or perhaps a small crater; either would be an expected consequence of the high-velocity ejection of pyroclasts during a Plinian eruption [Wilson et al., 1980].

Two scenarios for the eruption of bed 1 must now be considered. In the first scenario, the magma froth of bed 1 continued to be confined to a narrow dike until and during its eruption. In the second scenario, suggested by the existence of the graben between Northern Coulee and Upper Dome, the magma collected in a small elongate reservoir within the edifice of the volcano, a few tens of meters to several hundred meters beneath the ground surface, before being erupted as bed 1. In either scenario, the eruption probably began when the excess gas pressure in the magma froth finally exceeded the tensile strength and surface tension of the froth itself and the overburden pressure [Murase and McBirney, 1973].

Pulsating eruption from a dike. In a manner analogous to the initiation of basaltic fissure eruptions, the eruption may well have begun when a tensile crack or fissure above the shallow magma body opened to the ground surface, markedly decreasing the overburden pressure on the magma froth. As the froth began to fragment at the top of the magma body, rapidly expanding steam began to propel pyroclasts out of the fissure, and the "fragmentation surface" [Sparks, 1978] began to propagate downward.

If the erupting magma body was a dike, the downward velocity of the fragmentation surface (V_f) would be related to the rise velocity of the frothy magma (V_m), mass eruption rate ($\dot{m}$), density of the pyroclasts (ρ), and plan view area of the dike (A) by

$$V_f = \frac{\dot{m}}{\rho A} - V_m$$

The distribution of pyroclast sizes can be used to calculate the mass rate of eruption. Using the methods of Wilson [Wilson et al., 1978; L. Wilson, personal communication, 1985], we have calculated a mass rate of eruption for bed 1, $\dot{m} \sim 5 \times 10^9$ g/s. With reasonable values for ρ and A, the average downward velocity of the fragmentation surface can be calculated to have been ~20 cm/s relative to the bubbly liquid.

If this rate of downward propagation was an order of magnitude faster than the rate of buoyant rise of the viscous magma froth within the dike, the top of the magma froth would have experienced a net rate of drawdown in the dike nearly equal to the rate of downward propagation of the fragmentation surface. In this case, the fragmentation front would have reached a depth of 1 km, a few hundred meters above the initial depth of saturation of the bed 1 magma, within about 80 min of the beginning of the Plinian eruption of bed 1.

If, on the other hand, $\dot{m}/\rho A$ was about the same as V_m, then the fragmentation surface would not have propagated downward into the dike but would have remained at approximately the same level in the top of the dike.

The mechanism for ending the eruption of bed 1 in these scenarios is worth considering. Closure of the dike by normal faulting would be plausible if significant drawdown occurred in the dike but rather implausible if little drawdown occurred. Closure by normal faulting might happen because of the instability of the dike walls if the top of the magma dike was drawn down several hundred meters. This mechanism would require the pressure in bed 3-6 magma to be great enough to reopen the dike. Another plausible process for ending the eruption of bed 1 magma involves the dynamics of the gas/pyroclast mixture. Perhaps pyroclasts too large to be carried out of the crater by the gas fell back into the dike. As these particles accumulated, they would eventually have formed a thick pyroclastic "cap" over the magma which may have exerted enough of an overburden pressure to stop magma fragmentation and eruption [Wilson et al., 1980]. This "cap" would later be erupted from the dike as part of beds 3-6.

The eruption of bed 2 followed that of bed 1, but from a separate vent, source 3, now under Upper Dome. Assuming a dike length of 700 m, the drawdown for the eruption of bed 2 could have been as much as that of bed 1, about 1000 m. Cessation of the eruption of bed 2 could well have been by one of the same mechanisms proposed for bed 1. The next units, beds 3-6, were erupted from sources between Upper Dome and Northern Coulee. Downward propagation of the fragmentation surface during the Plinian eruption of these beds could have been as much as 900 m, judging from their vertical thickness in Figure 21. The possibility we are entertaining here is that bed 1, bed 2, and beds 3-6 each represents the fragmented volume of a vertical dike which repeatedly drew down to its initial water saturation depth of about 1000 m.

Pulsating eruption from a shallow, elongate cryptodome. The presence of the 600-m-wide graben between Northern Coulee and Upper Dome (Figure 15) suggests the possibility that at least a portion of the magma of the North Mono eruption was able to accumulate within the edifice at depths of less than 200 m. An accumulation of only about 0.01 km^3 of magma (two thirds the volume of bed 1) at a depth of about 200 m could explain the geometry and amount of throw on the graben faults. Data now available do not exclude the possibility that successive fillings and ventings of small, shallow cryptodomes such as that illustrated in Figure 16 occurred in the course of the North Mono eruption.

In such a scenario, one can imagine vesiculated magma of bed 1 accumulating as a shallow cryptodome beneath source 9 (Figure 16), well above its water saturation depth of 1500 m and with concomitantly large excess gas pressures. Eventually, fragmentation of the magma could have occurred in a fissure connecting the cryptodome with the surface, and the contents of the cryptodome could have been evacuated wholly or in part as the fragmentation front retreated into the cryptodome.

A pulsating eruption would be a logical consequence of this geometry. Partial evacuation of the cryptodome would lead to dip-slip movement on the graben faults (Figure 16b), which would choke off the fissure through which the magma froth was evacuating. Reinflation of the cryptodome by continued slow, buoyant rise of magma from the subjacent dike would gradually decrease normal stresses across the graben and eventually enable initiation of a second eruption of cryptodome magma. All the distinct Plinian and pyroclastic flow pulses might have been generated by repetition of this process.

Summary

Our field studies of the most recent eruption of the Mono Craters reveal that the North Mono eruption involved evacuation of 0.7 km^3 of pyroclastic debris and lava from several aligned vents along the northern crest of the volcanic chain. The eruption occurred between A.D. 1325 and 1365, and its more explosive phase lasted no more than several months.

The geometry of the vents indicates that the eruption resulted from intrusion of a 6-km-long, north-south trending dike into the shallow crust. Dike intrusions such as this appear to have replaced normal faulting as the dominant mechanism for crustal extension in this region. The diminishing explosiveness of the eruption as it progressed from Plinian to pyroclastic flow to extrusive phases is explained best as a result of stratification of water content in the magma dike.

Stratigraphic relationships clearly demonstrate that the North Mono eruption preceded the Inyo eruption of Miller [1985] but probably by no more than a few years. The near contemporaneity of these two eruptions suggests a causal relationship.

Acknowledgments. Spencer Wood first encouraged us to continue his unfinished work at the Mono Craters as a mapping project for an undergraduate summer field geology class in

1981. Scott Stine has been a wonderful source of information and enthusiasm during many conversations and field excursions. We were fortunate to be working in this area while he was discovering the Holocene stratigraphy of Mono Lake. Dan Miller's and Dan Sampson's recent discoveries to the south, in the Inyo volcanic chain and Pat Kelleher's study of the Mono Craters have also added to our enthusiasm for this work. Dave Stevenson tutored us in our attempt to understand the mechanism of the eruption. Conversations with Ari Fuad, Ed Stolper, and Sally Newman about their water content data also have helped us in attempting to understand the eruption. We are grateful for the assistance of Jim Drake, Pat Williams, Norm Brown, and Paul Haase in the field and to Paul Hawley and Jan Mayne for typing this manuscript and drafting most of the figures. Roy Bailey and Ken Cameron provided very helpful reviews of the manuscipt. Field work during the summers of 1982-1985 and radiocarbon dating were supported by generous donations from the Allan V.C. Davis Foundation. Part of M.B.'s field work in 1984 was supported by a Penrose grant (#3265-84) from the Geological Society of America. Caltech Division of Geological and Planetary Sciences Contribution number 4379.

References

Achauer, U., L. Greene, J. R. Evans, and H. M. Iyer, Evidence for a low-velocity body under Inyo/Mono Craters from the study of teleseismic P-wave residuals (abstract), Eos Trans. AGU, 65, 1116, 1984.

Axtell, L. H., Mono Lake geothermal wells abandoned, Calif. Geol., 25, 66-67, 1972.

Bailey, R. A., G. B. Dalrymple, and M. A. Lanphere, Volcanism, Structure, and Geochronology of Long Caldera, Mono County, California, J. Geophys. Res., 81(5), 725-744, 1976.

Carmichael, I. S. E., The iron-titanium oxides of salic volcanic rocks and their associated ferromagnesian silicates, Contrib. Mineral. Petrol., 14, 36-64, 1967.

Carmichael, I. S. E., F. J. Turner, and J. Verhoogen, Igneous Petrology, 739 p., McGraw-Hill, New York, 1974.

Curry, R. R., Glacial and Pleistocene History of the Mammoth Lakes Sierra--a geologic guidebook, Geol. Ser. Publ. 11, 52 p., Univ. of Mont., Dept. of Geol., Missoula, 1971.

Eichelberger, J. C., P. C. Lysne, C. O. Miller, and L. W. Younker, 1984 Drilling Results at Inyo Domes, California, EOS Trans. AGU, 66, 384, 1985.

Fink, J. H., Geometry of silicic dikes beneath the Inyo Domes, California, J. Geophys. Res., 90, 11,127-11,135, 1985.

Fink, J. H., and D. D. Pollard, Structural evidence for dikes beneath silicic domes, Medicine Lake Highland Volcano, California, Geology, 11, 458-461, 1983.

Fisher, R. V., and H. U. Schmincke, Pyroclastic Rocks, Springer-Verlag, New York, 1984.

Gilbert, G. K., A theory of earthquakes of the Great Basin with practical applications, Amer. J. Sci., 27, 49-53, 1884.

Gilbert, G. K., Studies of basin-range structures, U.S. Geol. Surv. Prof. Pap. 153, 1-92, 1928.

Hildreth, W., and G. A. Mahood, Ring-fracture eruption of the Bishop Tuff, Geol. Soc. Am. Bull., 97, 473-485, 1986.

Hill, D. P., R. A. Bailey, and A. S. Ryall, Active Tectonic and Magmatic Processes Beneath Long Valley Caldera, Eastern California: An Overview, J. Geophys. Res., 90, 11,111-11,120, 1985.

Huber, N. K., and C. D. Rinehart, Cenozoic volcanic rocks of the Devil's Postpile quadrangle, eastern Sierra Nevada, California, U.S. Geol. Surv. Prof. Pap. 554-D, 21 p., 1967.

Izett, G. A., and C. W. Naeser, Age of the Bishop Tuff of Eastern California as determined by the fission-track method, Geology, 4, 587-590, 1976.

Keefer, D. K., Landslides caused by earthquakes, Geol. Soc. Am. Bull., 95, 406-421, 1984.

Kelleher, P., The geology, petrology, and geochemistry of the Mono Craters-Mono Lake Islands volcanic complex, eastern California, M.S. thesis, Univ. of Calif,. Santa Cruz, 1986.

Kistler, R. W., Geologic map of the Mono Craters quadrangle, Mono and Tuolumne quadrangles, California, Map GQ-462, U.S. Geol. Surv., 1966.

Lachenbruch, A. H., J. H. Sass, R. J. Munroe, and T. H. Moses, Geothermal setting and simple heat conduction models for the Long Valley caldera, J. Geophys. Res., 81, 769-784, 1976.

Lajoie, K. R., Late Quaternary stratigraphy and geologic history of Mono Basin, Ph.D. thesis, 271 pp., Univ. of Calif., Berkeley, 1968.

Lajoie, K. R., and S. W. Robinson, Late Quaternary glacio-lacustrine chronology Mono Basin, California, Geol. Soc. Am., Abstr. Programs, 14, 179, 1982.

Lipman, P. W., Structure of the Tertiary Questa caldera, New Mexico--An eroded analog for current activity at Long Valley, Proceedings of Workshop XIX, Active Tectonic and Magmatic Processes Beneath Long Valley Caldera, Eastern California, vol. 2, U.S. Geol. Surv. Open File Rep., 84-939, 851-885, 1984.

Long, A. and B. Rippeteau, Testing contemporaneity and averaging radiocarbon dates, Am. Antiq., 39, 205-215, 1974.

Mayo, E. B., L. C. Conant, and J. R. Chelikowsky, Southern Extension of the Mono Craters, California, Am. J. Sci., 32, 81-97, 1936.

Metz, J., and G. Mahood, Precursors to the Bishop Tuff eruption: Glass Mountain, Long Valley, California, J. Geophys. Res., 90, 11,121-11,126, 1985.

Miller, C. D., Holocene eruptions at the Inyo volcanic chain, California: Implications for possible eruptions in Long Valley caldera, Geology, 13, 14-17, 1985.

Moore, J. G., K. Nakamura, and A. Alcaraz, The 1965 eruption of Taal volcano, Science, 151, 955-960, 1966.

Moore, J. G., P. W. Lipman, D. A. Swanson, and T. R. Alpha, Growth of lava domes in the crater, June 1980-January 1981, U.S. Geol. Surv. Prof. Pap., 1250, 541-547, 1981.

Murase, I., Viscosity and related properties of volcanic rocks at 800° to 1400°C, J. Fac. Sci. Hokkaido Univ., Ser. 7, 1, 487-584, 1962.

Murase, I., and A. R. McBirney, Properties of some common igneous rocks and their melts at high temperatures, Geol. Soc. Am. Bull., 84, 3563-3592, 1973.

Newman, S., E. M. Stolper, and S. Epstein, Measurement of water in rhyolitic glasses: calibration of an infrared spectroscopic technique, Am. Mineral., in press, 1986.

Pollard, D. D., J. H. Fink, and P. T. Delaney, Igneous dikes at Long Valley, CA: Emplacement mechanisms and associated geologic structures: Proceedings of Workshop XIX, Active Tectonic and Magmatic Processes Beneath Long Valley, Eastern California, vol. 1, U.S. Geol. Surv. Open File Report 84-939, 130-146, 1984.

Putnam, W. C., The Mono Craters, California, Geogr. Rev., 28, 68-82, 1938.

Reid, H. F., The California earthquake of April 18, 1906, The mechanics of the earthquake, Report of the (California) State Earthquake Investigation Commission, Carnegie Institute of Washington, Pub. no. 87, v. 2, p. 1-192, 1910.

Rinehart, C. D., and N. K. Huber, The Inyo Crater Lakes--A blast in the past, Calif. Div. of Mines and Geol., Miner. Inf. Serv., 18, pp. 169-172, Sacramento, 1965.

Russell, I. C., Quaternary history of the Mono Valley, California, Eighth Annu. Rep., pp. 267-394, U.S. Geological Survey, Reston, Va., 1889.

Salyards, S. L., Thermal and depositional constraints on a block and ash flow deposit from Panum Crater, Mono Co., California, from paleomagnetic analysis, Geol. Soc. Am. Abstr. Programs, 18, 180, 1986.

Sarna-Wojcicki, A. M., S. Shipley, R. B. Waitt, Jr., D. Dzurisin, and S. H. Wood, Areal distribution, thickness, mass, volume, and grain xize of air-fall ash from the six major eruptions of 1980: Washington, U.S. Geol. Surv. Prof. Pap. 1250, 577-600, 1981.

Savage, J. C., Strain accumulation in western United States, Annu. Rev. Earth Planet. Sci., 11, 11-43, 1983.

Scott, W. E., Character and age of Holocene rhyodacite eruptions at South Sister volcano, Oregon, Eos Trans. AGU, 64, 899-900, 1983.

Shaw, H. R., Comments on viscosity, crystal settling, and convection in granitic magmas, Am. J. Sci., 263, 120-152, 1965.

Shaw, H.R., Diffusion of H_2O in granitic liquids, part I, Experimental data; part II, Mass transfer in magma chambers, Geochemical transport and kinetics, edited by A. W. Hofmann, B. J. Giletti, H. S. Yoder, Jr., and R. A. Yund, Carnegie Inst. Washington Publ., 634, 139-170, 1974.

Simpkin, T., and R. S. Fiske, Krakatau, 1883, 464 p., Smithsonian Institution Press, Washington, D.C., 1983.

Sims, J. D., Earthquake-induced structures in sediments of Van Norman Lake, San Fernando, California, Science, 182, 161-163, 1973.

Smith, E. I., Mono Craters, California: A new interpretation of the eruptive sequence, Geol. Soc. Am. Bull., 84, 2685-2690, 1973.

Sparks, R. S. J., The dynamics of bubble growth and formation in magmas: A review and analysis, J. Volcanol. Geotherm. Res., 3, 1-37, 1978.

Sparks, R. S. J., H. Sigurdsson, and L. Wilson, Magma mixing: A mechanism for triggering acid explosive eruptions, Nature, 267, 315-318, 1977.

Stein, R. S., and S. E. Barrientos, The 1983 Borah Peak, Idaho, earthquake: Geodetic evidence for deep rupture on a planar fault, in Proceedings of Workshop XXVIII, On the Borah Peak, Idaho, Earthquake, vol. A, pp. 459-484, U.S. Geol. Surv., 1985.

Stine, S., Late Holocene lake level fluctuations and island volcanism at Mono Lake, California, Geologic Guide to Aspen Valley, Mono Lake, Mono Craters, and Inyo Craters, pp. 21-49, Genny Smith Books, Palo Alto, Calif., 1984.

Stolper, E., Water in silicate glasses: An infrared spectroscopic study, Contrib. Mineral. Petrol., 81, 1-17, 1982.

Stuiver, M., A high-precision calibration of the A.D. radiocarbon time scale, Radiocarbon, 24, 1-26, 1982.

Stuiver, M., and H. A. Polach, Discussion reporting of ^{14}C data, Radiocarbon, 3, 355-363, 1977.

Taylor, B. E., J. C. Eichelberger, and H. R. Westrich, Hydrogen isotopic evidence of rhyolitic magma degassing during shallow intrusion and eruption, Nature, 306, 541-545, 1983.

Turcotte, D., and G. Schubert, Geodynamics, 450 pp., John Wiley, New York, 1982.

Waitt, R. B., V. L. Hanson, A. M. Sarna-Wojcicki, and S. H. Wood, Proximal air-fall deposits of eruptions between May 24 and August 7, 1980 - Stratigraphy and field sedimentology, U.S. Geol. Surv. Prof. Pap., 1250, 617-628, 1981.

Walker, G. P. L., The Taupo Pumice: Product of the most powerful known (ultraPlinian) eruption?, J. Volcanol. Geotherm. Res., 8, 69-94, 1980.

Wallace, R. E., Active faults, paleoseismology, and earthquake hazards in the western United States, Earthquake Prediction--An International Review, Maurice Ewing Ser., vol. 4, edited by D. W. Simpson and P. G. Richards, pp. 209-216, AGU, Washington, D.C., 1981.

Whitten, C. A., The Dixie Valley-Fairview Peak, Nevada, earthquakes of December 16, 1954: Geodetic measurements, Bull. Seismol. Soc. Am., 47, 321-325, 1957.

Williams, H., and A. R. McBirney, Volcanology, 397 pp., Freeman, Cooper, San Francisco, Calif., 1979.

Wilson, L., R. S. J. Sparks, T. C. Huang, and N. D. Watkins, The control of volcanic column heights by eruption energetics and dynamics, J. Geophys. Res., 83, 1829-1836, 1978.

Wilson, L., R. S. J. Sparks, and G. P. L. Walker, Explosive volcanic eruptions, IV, The control of magma properties and conduit geometry on eruption column behavior, Geophys. J. R. Astron. Soc., 63, 117-148, 1980.

Wohletz, K., and M. Sheridan, Hydrovolcanic explosions, II, Evolution of basaltic tuff rings and tuff cones, Am. J. Sci., 283, 383-413, 1983.

Wood, S. H., Chronology of Late Pleistocene and Holocene volcanics, Long Valley and Mono Basin

geothermal areas, eastern California, technical report, contract 14-08-0001-15166, U.S. Geol. Surv., 1977a (reprinted as U.S. Geol. Surv. Open File Rep., 83-747, 76 pp., 1983.)

Wood, S. H., Distribution, correlation, and radiocarbon dating of Late Holocene tephra, Mono and Inyo Craters, eastern California, Geol. Soc. Am. Bull., 88, 89-95, 1977b.

Wood, S. H., Obsidian hydration-rind dating of the Mono Craters, in Geologic Guide to Aspen Valley, Mono Lake, Mono Craters, and Inyo Craters, pp. 82-87, Genny Smith Books, Palo Alto, Calif., 1984.

Wood, S. H., and S. Stine, Mono Lake County Park at Dechambeau Creek, in Geologic Guide to Aspen Valley, Mono Lake, Mono Craters, and Inyo Craters, pp. 50-52, Genny Smith Books, Palo Alto, Calif., 1984.

Wood, S. H., M. P. Doukas, S. Shipley, R. B. Waitt, A. Sarna-Wojcicki, J. E. Vallance, and A. Eggers, The July 22, 1980 eruption of Mount St. Helens: Characteristics of the eruption and air-fall tephra, U.S. Geol. Surv. Prof. Pap. 1251, in press, 1986

Youd, T. L., and D. M. Perkins, Mapping of liquefaction-induced ground failure potential, J. Geotech. Eng. Div. Am. Soc. Civ. Eng., 104(GT4), 443-446, 1978.

M. Bursik and K. Sieh, Division of Geological and Planetary Sciences, California Institute of Technology, Pasadena, CA 91125.

(Received January 14, 1986;
revised June 4, 1986;
accepted June 23, 1986.)